Mon. Not. R. Astron. Soc. **000**, 000–000 (0000) Printed 1 February 2008 (MN LaTeX style file v2.2)

arXiv:astro-ph/0207360v1 17 Jul 2002

Galaxy Properties in Low X-Ray Luminosity Clusters at z=0.25

Michael Balogh[1,2], R. G. Bower[1,4], Ian Smail[1], B. L. Ziegler[3,4], Roger L. Davies[1], A. Gaztelu[1], Alexander Fritz[3]
[1] *Department of Physics, University of Durham,South Road, Durham DH1 3LE, UK*
[2] *email: M.L.Balogh@Durham.ac.uk*
[3] *Universitaetssternwarte, Geismarlandstr. 11, 37083 Goettingen, Germany*
[4] *Visiting astronomer of the German–Spanish Astronomical Center, Calar Alto, operated by the Max–Planck–Institut für Astronomie, Heidelberg, jointly with the Spanish National Commission for Astronomy.*

1 February 2008

ABSTRACT
We present the first spectroscopic survey of intrinsically low X-ray luminosity clusters at $z \gg 0$, with *Hubble Space Telescope (HST)* WFPC2 imaging and spectroscopy from Calar Alto and WHT-LDSS2. We study 172 confirmed cluster members in a sample of ten clusters at $0.23 < z < 0.3$, with $L_X \lesssim 4 \times 10^{43} h^{-2}$ ergs s^{-1} [0.1-2.4 keV] ($\Omega_m = 0.3, \Lambda = 0.7$). The core of each cluster is imaged with WFPC2 in the F702W filter, and the spectroscopic sample is statistically complete to $M_r \sim -19.0 + 5\log h$, within an $11'$ (~ 1.8 h^{-1} Mpc) field. The clusters are dynamically well-separated from the surrounding field and most have velocity distributions consistent with Gaussians. The velocity dispersions range from ~ 350–850 km s^{-1}, consistent with the local $L_X-\sigma$ correlation. All ten clusters host a bright, giant elliptical galaxy without emission lines, near the centre of the X-ray emission. We measure the equivalent width of two nebular emission lines, [OII] and Hα, and the Hδ absorption line to spectrally classify the cluster members. Galaxy morphologies are measured from the *HST* images, using the two-dimensional surface-brightness fitting software GIM2D. Emission line galaxies in these clusters are relatively rare, comprising only 22±4% of the sample. There is no evidence that these emission-line galaxies are dynamically distinct from the majority of the cluster population, though our sample is too small to rule out the ~ 30% difference that has been observed in more massive clusters. We find eleven galaxies, comprising 6% of the cluster members, which are disk-dominated but show no sign of emission in their spectrum. Most of these are relatively isolated, spiral galaxies with smooth disks. We find no cluster members with a starburst or post-starburst spectrum. The striking similarity between the spectral and morphological properties of galaxies in these clusters and those of galaxies in more massive systems at similar redshifts implies that the physical processes responsible for truncating star formation in galaxies are not restricted to the rare, rich cluster environment, but are viable in much more common environments. In particular, we conclude that ram pressure stripping or cluster-induced starbursts cannot be solely responsible for the low star formation rates in these systems.

Key words: galaxies: clusters

1 INTRODUCTION

The evolutionary history of galaxies depends both on cosmic time and on the type of environment in which they exist. For example, recent studies have shown that the universal average star formation rate (SFR) has been declining steadily since at least $z \sim 1$ (Lilly et al. 1996; Madau et al. 1996; Cowie et al. 1999; Wilson et al. 2002). In a somewhat analogous way, star formation rates are known to monotonically decrease with increasing density at a given epoch (e.g. Balogh et al. 1997; Poggianti et al. 1999; Lewis et al. 2002). In both cases, the reason for the decrease in star formation is unknown. In particular, there is plenty of gas still available for star formation at the present day, so the sharp decline in activity over the past ~ 5 Gyr is a critical issue. It is an intriguing possibility that the processes which influence the evolution of galaxies that end up in dense clusters may be more generally important to galaxies in other, more common, environments. If this is so, it may be possible to link the decline in the universal average star formation rate to environmental effects in a Universe which is growing hierarchically.

We now have a good empirical description for the galaxy populations of massive clusters. Galaxies within the virial radius have, on average, lower star formation rates, and less recent (< 1Gyr) star formation, than galaxies in the surrounding field; this is true both locally (Lewis et al. 2002; Gomez et al. 2002) and at higher redshifts (e.g. Couch & Sharples 1987; Balogh et al. 1997, 1999; Poggianti et al. 1999; Postman et al. 2001; Couch et al. 2001; Balogh et al. 2002a). Evidence is mounting that this deficiency in star formation activity is at least partially independent of the morphology-density relation (Dressler et al. 1997; Balogh et al. 1998; Poggianti et al. 1999; Couch et al. 2001; Lewis et al. 2002; Gomez et al. 2002). However, an explanation for this difference between cluster and field galaxies is still lacking. Ram pressure stripping of cold gas in the disk of a galaxy (Gunn & Gott 1972; Fujita 1998; Quilis et al. 2000) is only likely to take place in the dense cores of rich clusters, and it seems unlikely that it can explain the suppression of star formation as far as several Mpc from the centre (Balogh et al. 1997; Kodama et al. 2001). Galaxy harassment (Moore et al. 1999) may be effective at destroying small galaxy disks, but the effect that this will have on the star formation rate of the galaxy is not clear. On the other hand, the observed radial and density dependences of galaxy stellar populations and morphologies are reproduced quite well by hierarchical models in which only the diffuse, hot halo gas expected to surround isolated galaxies is stripped (Larson et al. 1980; Balogh et al. 2000; Diaferio et al. 2001; Okamoto & Nagashima 2001; Bekki et al. 2002). The observed increase in activity with redshift is most likely a consequence of the higher infall rate (Bower 1991; Ellingson et al. 2001; Kodama & Bower 2001), though projection effects may still play a role (Diaferio et al. 2001).

For most cluster galaxies, the last episode of star formation occurred many billions of years ago. Thus, if some physical mechanism is responsible for the transition from a more active state, it must have occurred in the distant past, and will be difficult to uncover by observing galaxies in their present state (e.g. Trager et al. 1998; de Jong & Davies 1997; Kewley et al. 2001). It is therefore necessary to consider how the galaxy populations have evolved over time (Butcher & Oemler 1984; Dressler et al. 1999; Kodama & Smail 2001; Kodama & Bower 2001). However, in hierarchical models of galaxy formation, the progenitors of today's most massive clusters are expected to be numerous smaller structures at higher redshifts (e.g., Kauffmann 1996). Thus, galaxies must be observed not only over a range of redshifts, but for a range of cluster masses as well.

For this purpose we have carried out an extensive observational campaign to obtain *Hubble Space Telescope (HST)* imaging and ground-based imaging and spectroscopy for ten clusters at $z \approx 0.25$, selected to have low X-ray luminosities (hereafter referred to as the Low–L_X sample). This sample can be directly compared with studies of more massive clusters, both locally (Lewis et al. 2002; Gomez et al. 2002) and at higher redshift (Balogh et al. 1997; Smith et al. 2002). For example, in Balogh et al. (2002b, hereafter Paper I) we presented an analysis of the *HST* data for the present cluster sample, and compared it with a similar *HST* sample of high X-ray luminosity cluster cores. We found marginal ($\sim 2\sigma$) evidence that the Low–L_X clusters have more disk-dominated galaxies at a fixed local density. This suggests that at least galaxy morphology is sensitive to the large-scale structure. In the present paper we will revisit this, and other issues, in light of the spectroscopic data.

The paper is organized as follows. In § 2 we present the cluster selection, and the data acquisition, reduction and analysis. Our results are presented in § 3, where we consider the dynamics and spectral properties of the galaxy population. In § 4 we compare our results with those found for more massive clusters, and consider the implications of these results for models of galaxy evolution. We summarize our findings in § 5. We use a cosmology with $\Lambda = 0.7$, $\Omega_m = 0.3$, and parametrise the Hubble constant as $H_\circ = 100h$ km s^{-1} Mpc^{-1}.

2 OBSERVATIONS, REDUCTION AND ANALYSIS

2.1 Cluster Selection

The cluster sample is the same as the Low–L_X sample analysed in Paper I, with the addition of Cl 1633+57, comprising ten X-ray faint clusters in the northern hemisphere[1]. The clusters are selected from the sample identified by Vikhlinin et al. (1998) in serendipitous, pointed *ROSAT PSPC* observations, restricted to a relatively narrow redshift range, $z = 0.22$–0.29 ($\sigma z/z \sim 0.1$) and a mean redshift of $z = 0.25$, to reduce the effects of differential distance modulus and k-correction effects on the comparison between the systems. We compute $L_{\rm X}$ in the 0.1–2.4 keV band from the observed fluxes in the 0.5–2.0 keV band, corrected for galactic HI absorption and assuming a k-correction appropriate for an intra-cluster gas temperature equal to that expected from the local $L_{\rm X} - kT$ relation (Allen & Fabian 1998; Markevitch 1998), using the software package XSPEC. These luminosities are listed in Table 1, and range from 0.40 to $4.0 \times 10^{43} h^{-2}$ ergs s^{-1}[0.1–2.4 keV] (Table 1). Although Cl 1444+63 is treated as two separate clusters, the X-ray luminosity in Table 1 is that of the combined clusters.

2.2 Imaging and Spectroscopy

HST imaging with *WFPC2* is available for all clusters in the sample. The observations of all clusters but Cl 1633+57 are described more completely in Paper I. To summarize, each cluster was observed with three single orbit exposures in the F702W filter during Cycle 8. The photometry is calibrated on the Vega system, with updated zero points taken from the current instrument manual. The final images reach a 3-σ point source sensitivity of $R_{702} \sim 25.5$, and cover a field of $2.5' \times 2.5'$ (or $0.4h^{-1}$ Mpc at $z = 0.25$) with an angular resolution of $0.17''$ ($\sim 0.5h^{-1}$ kpc). The cluster Cl 1633+57

---

[1] The cluster Cl 1444+63 turns out to be two clusters aligned along the line of sight (see § 2.3), and we consider the two clusters separately.

Table 1. PROPERTIES OF THE TEN CLUSTERS

Name	R.A. (J2000)	Dec. (J2000)	N_{memb}	$< z >$	σ (km/s)	L_{X} (0.1–2.4 keV) $10^{43}h^{-2}$ ergs s^{-1}	Completeness[a]
Cl 0818+56	08 19 04	+56 54 49	9	0.2670	651±165	1.50	0.66
Cl 0819+70	08 19 18	+70 55 48	23	0.2296	356±39	1.26	0.88
Cl 0841+70	08 41 44	+70 46 53	21	0.2397	399±170	1.22	0.52
Cl 0849+37	08 49 11	+37 31 09	26	0.2343	764±90	1.93	0.69
Cl 1309+32	13 09 56	+32 22 14	19	0.2932	662±1304	2.01	0.41
Cl 1444+63a	14 43 55	+63 45 35	13	0.2923	403±73	3.99[b]	0.49
Cl 1444+63b	14 44 07	+63 44 59	15	0.3006	449±681	3.99[b]	0.49
Cl 1633+57	16 33 42	+57 14 12	18	0.2402	582±360	0.49	0.87
Cl 1701+64	17 01 47	+64 20 57	12	0.2458	834±647	0.40	0.52
Cl 1702+64	17 02 14	+64 19 53	15	0.2233	386±426	0.74	0.52

[a] Computed for galaxies more than 1 magnitude brighter than the faintest galaxy with a redshift in that cluster.
[b] Cl 1444+63 is only detected as a single X-ray source; this L_{X} presumably includes contribution from both clusters.

was observed in Cycle 8 (Proposal ID 7374), and the data were retrieved from the CADC[2] *HST* archive. These data are F702W WFPC2 observations, with four exposures of 1200 seconds. The total exposure time of 4800 seconds is therefore less than that of the other nine clusters (typically 7000 seconds; see Paper I). The calibrated images obtained from the CADC were combined in the same way as described in Paper I.

The spectroscopic sample is selected from ground-based imaging from the Palomar 200-inch telescope and the Isaac Newton telescope (INT) . The single INT Wide-Field Camera (WFC) chip from which the galaxies were selected covers 11.4′ at 0.″33 arcsec pix^{-1}, while the Palomar COSMIC images have a field-of-view of 13.7′with a pixel scale of 0.″4 arcsec pix^{-1} (Kells et al. 1998). For all but two clusters, galaxies were selected for spectroscopic follow-up from the $R-$band images. In Cl 1309+32 and Cl 1444+63 the sample was selected from $I-$band images, because R was not available. Note that the two clusters Cl 1701+64 and Cl 1702+64 are sufficiently close together that spectroscopic targets for both could be selected from a single WFC chip. The conditions during the imaging observations were not photometric, so we have calibrated our images by comparing aperture magnitudes of several (usually 2-3) relatively isolated, early-type galaxies with the F702W photometry of the *WFPC2* images, and converted this to standard R magnitudes, assuming $R_{\mathrm{F702W}} - R_c = -0.2$ (Fukugita et al. 1995). Because of uncertainties in the colour term, and the small number of calibration galaxies used for each cluster, the photometric calibration is likely to be accurate to only ~ 0.2 mag.

The spectra were obtained over four observing runs, and we give a log of these in Table 2. Three sets of data were taken with MOSCA on the 3.5-m telescope at Calar Alto Observatory, using the g500 grism. The spectra have a dispersion of $\sim$ 2.7Å pix^{-1} and cover 4000Å−8000Å, with a resolution of $\sim 10 - 15$Å. The fourth observing run was with LDSS-2 on the William Herschel Telescope. Using the medium-blue grism, we obtained a dispersion of $\sim$ 4.5Å pix^{-1}, covering 3500–9000Å. The resolution of these spectra is $\sim$ 15–20Å. Typically, two masks were observed for each cluster; in some cases a third mask was also obtained. Galaxies were selected for spectroscopic follow up based solely on their instrumental R or I band magnitude, with preference given to brighter galaxies. The fraction of galaxies observed spectroscopically therefore declines toward fainter magnitudes. For each mask we obtain between 20 and 35 spectra through 1.″5 wide slits, over an 11′ field of view. In total we obtained 581 spectra, in variable conditions. Some galaxies observed in poor conditions were later reobserved in a subsequent run. We obtained reliable redshifts for a total of 317 galaxies, of which 172 are cluster members. A summary of the photometric and spectroscopic observations is given in Table 2.

2.3 Data Reduction and Analysis

The spectroscopic data were reduced using IRAF[3] software. The images were bias-subtracted and median-combined to remove cosmic rays. Spectra were optimally extracted and the sky was subtracted by fitting a one- or two-degree polynomial to the counts on either side of the object. The spectrum was traced along the dispersion direction of the CCD to account for distortion. Wavelength calibration was based on either HgNeAr arc lamps or emission lines in the night-sky spectrum; the latter method was generally used to improve the calibration at the red end of the spectrum. The *r.m.s.* of the wavelength solution is typically $\lesssim 1$Å for $\lambda \lesssim 7000$Å, corresponding to $\Delta z \lesssim 2 \times 10^{-4}$. The spectra were not flat-fielded or flux calibrated, which is inconsequential for this analysis since we restrict our attention to spectral features that are defined relative to the continuum, over a narrow wavelength range ($\sim$ 150Å).

Galaxy redshifts were determined by three of us (MLB, BLZ, AF), each with an independent method. MLB used the routine FXCOR within the IRAF environment to cross-correlate the spectra with high signal-to-noise $z = 0$ galaxy

---

[2] Canadian Astronomy Data Centre, which is operated by the Herzberg Institute of Astrophysics, National Research Council of Canada.

[3] IRAF is distributed by the National Optical Astronomy Observatories which is operated by AURA Inc. under contract with NSF.

Table 2. Log of Observations

Name	Instrument	Date	Band (phot) $N_{\rm mask}$/ $N_{\rm spec}$	$T_{\rm exp}$ (ks)
Cl 0818+56	COSMIC	26/11/98	R	0.3
	MOSCA	04/02/00	2 / 53	7.2
	LDSS2	02/03/00	2 / 53	5.4/7.2
Cl 0819+70	COSMIC	26/11/98	R	0.25
	MOSCA	03/11/00	2 / 39	7.2
	LDSS2	04/03/00	1 / 21	7.2
Cl 0841+70	COSMIC	26/11/98	R	0.25
	MOSCA	04/02/00	2 / 31	7.2
	LDSS2	05/03/00	1 / 21	7.2
Cl 0849+37	COSMIC	26/11/98	R	0.25
	MOSCA	14/04/99	1 / 29	5.4
	MOSCA	05/02/00	2 / 41	7.2/9.6
Cl 1309+32	INT/WFC	19/06/98	I	0.6
	MOSCA	12/04/99	2 / 89	7.2/9.0
	MOSCA	05/02/00	1 / 31	9.6
Cl 1444+63	INT/WFC	18/01/99	I	0.72
	MOSCA	13/04/99	1 / 31	9.0
	MOSCA	06/02/00	1 / 36	7.2
Cl 1633+57	INT/WFC	10/02/99	R	0.6
	MOSCA	12/04/99	2 / 58	7.2
Cl 1701+64/ Cl 1702+64	INT/WFC MOSCA	10/02/99 30/07/00	R 2 / 48	0.6 5.4

spectral templates of similar resolution. BLZ used the Fourier Correlation Quotient (Bender 1990) within MIDAS, which compares absorption lines with those of template stars, while AF measured the centroids of several prominent absorption lines. The agreement between the three measurements is good, and generally within the uncertainty (typically $\sim$ 100 km s^{-1}). The independent estimates allowed us to identify galaxies where one method failed (because of low signal-to-noise ratio around a critical line, for example). Spectra for which we could not resolve the discrepancy between different redshift estimates ($\lesssim 5\%$) were always of low signal-to-noise ratio, and were removed from further analysis.

In Figure 1 we show the distribution of signal-to-noise ratio per resolution element, including only those spectra for which a redshift was obtained. The S/N is computed in the rest-frame continuum region 4050–4250Å, redward of the 4000Å break, and has a median of $\sim$ 10 per resolution element. It can easily be shown that, for spectra with a resolution of 15 Å, an emission line can be measured with an uncertainty < 5 Å if $S/N > \sqrt{18 + (W/5)^2}$, where W is the equivalent width of the line, assuming the uncertainty is dominated by the continuum flux (true for weak lines). Thus, lines as weak as $W \sim 5$Å can be reliably measured if $S/N > 4.3$Å, which is satisfied by $\sim$90% of our spectra.

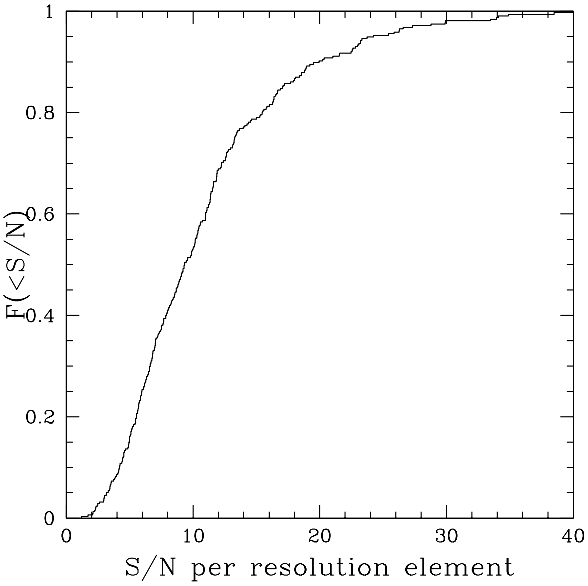

Figure 1. The cumulative distribution of signal-to-noise ratio per resolution element, for the 315 galaxies in our sample with redshifts. The resolution element is $\sim$ 15Å for the MOSCA spectra, and $\sim$ 20Å for the LDSS-2 spectra.

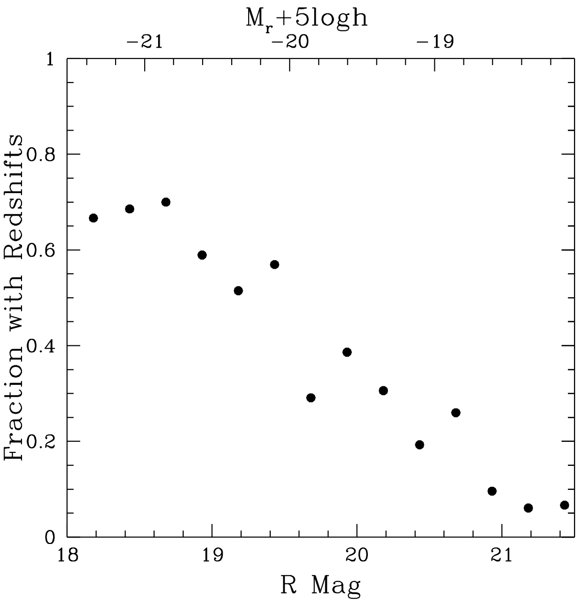

Figure 2. The average selection function for the whole sample. The top axis shows the k-corrected luminosity for a cluster at z=0.25. In practice, the data are weighted by the selection function, as a function of instrumental magnitude, for each cluster separately.

2.4 Selection Function and Magnitude Limits

For each cluster, we determine the fraction of galaxies in the photometric catalogue for which a redshift was obtained, as a function of instrumental magnitude. Galaxies in our spectroscopic sample are then weighted by the inverse of this selection function to obtain a sample which is statistically magnitude limited. The selection function is determined separately for each cluster, as a function of instrumental magnitude. In Figure 2 we show the combined selection function for the full sample, as a function of $R-$magnitude. We define the completeness as the fraction of galaxies with a redshift

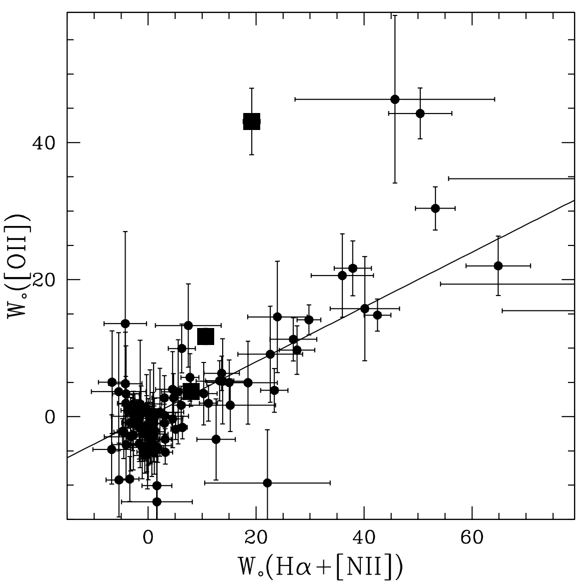

Figure 3. The correlation between $W_\circ(H\alpha$+[Nii]$)$ and $W_\circ$([Oii]) for galaxies in which a reliable measurement of both lines exists. Error bars are $1-\sigma$. The three galaxies represented by *filled squares* have strong, broad [Nii] emission characteristic of non-thermal emission. The solid line is the average local relation measured by Kennicutt (1992). Three points are off the scale, at $W_\circ(H\alpha$+[Nii]$)>$ 80Å; part of the error bars are just visible.

in each cluster field, considering only galaxies brighter than 1 magnitude above the faintest galaxy for which a redshift was obtained. This quantity is tabulated in Table 1.

Our sample is $\gtrsim 20$% complete at $R \sim 20.5$, which corresponds to $M_R \sim -19.0 + 5\log h$ at $z = 0.25$ (including a k-correction of 0.2 mag). Unless otherwise stated, we limit our sample to galaxies brighter than this magnitude, which corresponds to ∼2 magnitudes fainter than M^*.

2.5 Line Index Measurements

We have shown that the signal-to-noise ratio and resolution of our spectra are sufficient to allow us to reliably measure spectral features with equivalent widths $W \gtrsim$ 5Å. In particular we focus on the rest frame equivalent width of the [Oii]λ3727 emission line, which is a signature of gas ionized by hot stars and, hence, the best indicator of current star formation in the blue region of the spectrum (e.g., Kennicutt 1983). However, it is less than perfect for several reasons. Perhaps most importantly, it is a weak line, usually with an equivalent width $<$ 30Å. In moderate signal-to-noise spectra like ours, therefore, it is difficult to detect low levels of star formation. Furthermore, the equivalent width of [Oii] is sensitive to metallicity and the ionization level of the gas (Charlot & Longhetti 2001; Charlot et al. 2002), which can introduce a scatter in the [Oii]-SFR relation of a factor $\gtrsim 5$. Finally, it seems likely that the Hii regions where [Oii] is produced will be more heavily obscured than the longer-lived stars which give rise to the continuum (e.g. Silva et al. 1998; Charlot & Fall 2000). In this case, the equivalent width will underestimate the star formation rate, even if a global extinction correction is applied. However, despite these difficulties, it has been shown that [Oii] correlates with better star formation indicators like Hα emission (Kennicutt 1992; Jansen et al. 2000, also see Fig 3). Although there is a large scatter in this correlation, the average star-formation properties of a population can be well-described.

We also measure the Hδ absorption line, which is a strong feature in A-stars and thus represents recent star formation. As this is an absorption feature, and affected by emission-filling, its precise measurement is more difficult than that of the emission lines, and little can be said about most of the galaxy population. However, galaxies with very strong Hδ absorption are easily detected, and these galaxies may play an important role in galaxy evolution (Dressler & Gunn 1983; Couch & Sharples 1987; Poggianti et al. 1999; Balogh et al. 1999).

These rest-frame equivalent widths are measured by fitting a line to the continuum on either side of the feature, and summing the flux above this continuum over a well-defined wavelength range. The definitions of the $W_\circ$([Oii]) and $W_\circ(H\delta)$ indices are the same as in Balogh et al. (1999)[4]. We will adopt the convention that $W_\circ$([Oii]) is positive when in emission, and $W_\circ(H\delta)$ is positive in absorption. Each line measured is checked to ensure that the continuum fit or spectral line pixels are not adversely affected by bad sky subtraction, bad pixels, or poor wavelength calibration. This removes 7.8% of the cluster member [Oii] measurements from our analysis. Uncertainties are computed as described in Balogh et al. (1999), and include the Poisson noise contributed from the sky subtraction and, therefore, the degradation effected by the spectral resolution.

There are 167 cluster members with reliable measurements of [Oii], and 107 of these also have reliable measurements (not necessarily detections) of Hα+[Nii]. Thus, we can use measurements of this line to check the reliability of [Oii] as a star formation indicator in this sample. We measure $W_\circ(H\alpha$+[Nii]$)$ in a manner analogous to that for $W_\circ$([Oii]), by computing the flux in the range 6555Å$< \lambda <$ 6575Å, compared with the continuum in the regions 6490Å$< \lambda <$ 6537Å and 6594Å$< \lambda <$ 6640Å. We do not deblend the two adjacent [Nii] lines, but include them both in the equivalent width measurement. The [Nii]λ6548 line always contributes only a small amount of flux ($<$ 5%), while the stronger [Nii]λ6583 line contributes $\sim$ 30% of the flux. The observed correlation between $W_\circ(H\alpha$+[Nii]$)$ and $W_\circ$([Oii]) is in excellent agreement with the local field correlation of Kennicutt (1992), as shown in Figure 3. Galaxies for which $W_\circ$([Oii])$>$ 5Å are almost always detected with $W_\circ(H\alpha$+[Nii]$)>$ 20Å. Only three (4%) of these galaxies have strong, broad [Nii]λ6583 indicating that their emission is dominated by non-thermal processes (Veilleux & Osterbrock 1987; Kewley et al. 2001).

2.6 Morphologies

There are 78 galaxies for which we have both spectroscopy and *HST WFPC2* imaging; 62 of these are confirmed cluster

---

[4] Note that the $W_\circ(H\delta)$ feature wavelength range given in Table 1 of Balogh et al. (1999) is incorrect. In both that work and the present analysis, the feature is taken to cover 4088–4116Å.

Table 3. Fraction of Disk Galaxies

Cluster	$F_{\rm stat}$ ($R<23$) (Paper I)	$F_{\rm stat}$ ($R<20$)	$F_{\rm spec}$
Cl 0818+56	0.43±0.08	0.64±0.17	0.56±0.38
Cl 0819+70	0.15±0.37	0.07±0.23	0.00±0.10
Cl 0841+70	0.36±0.27	0.04±0.12	0.00±0.05
Cl 0849+37	0.45±0.10	0.22±0.12	0.14±0.17
Cl 1309+32	0.37±0.09	0.36±0.15	0.14±0.17
Cl 1444+63	0.23±0.10	0.20±0.12	0.20±0.20
Cl 1633+57	0.26±0.18	0.17±0.18	0.00±0.10
Cl 1701+64	0.50±0.10	0.36±0.16	0.32±0.25
Cl 1702+64	0.47±0.12	0.42±0.19	0.00±0.14

members (see § 3.1 for the membership definition). As described in Paper I, we have measured fractional bulge luminosities, B/T, from these images using the two-dimensional surface brightness-fitting software package GIM2D (Simard et al. 2002). The *HST* imaging only covers the central ~ 0.6 Mpc in these clusters, and the number of disk-dominated, confirmed cluster members is small: only eight galaxies ($18 \pm 5\%$) brighter than $R = 20$ have $B/T < 0.4$. This is much less than the $\sim 40\%$ fraction of disk-dominated galaxies found in Paper I. This difference can be attributed to the different limiting magnitudes of the two analyses. The present spectroscopic sample is limited to $R \sim 20$, while in Paper I we considered a sample three magnitudes fainter, using only the *HST* imaging data. In Table 3 we list as $F_{\rm stat}$ the fraction of disk galaxies ($B/T < 0.4$) for each cluster, with a statistical background subtraction based on the Medium Deep Survey (Ostrander et al. 1998; Ratnatunga et al. 1999, see Paper I for details). We show both the value computed to $R \sim 23$, as published in Paper I, and the value considering only galaxies with $R < 20$. These numbers are compared with $F_{\rm spec}$, the fraction of disk-dominated galaxies determined from the spectroscopic sample of cluster members, complete to $R \lesssim 20$ (we combine the two clusters Cl 1444a and Cl 1444b to be consistent with the measurement of $F_{\rm stat}$). The errors are all computed from bootstrap resampling, except in the case where no disk galaxies are found, where we assume a Poisson distribution. Adopting the brighter limit appropriate for our spectroscopic sample, the fraction of disks determined by photometric field correction is 26±17%. This number is consistent with the spectroscopically-determined number ($18 \pm 5\%$), within the statistical uncertainties.

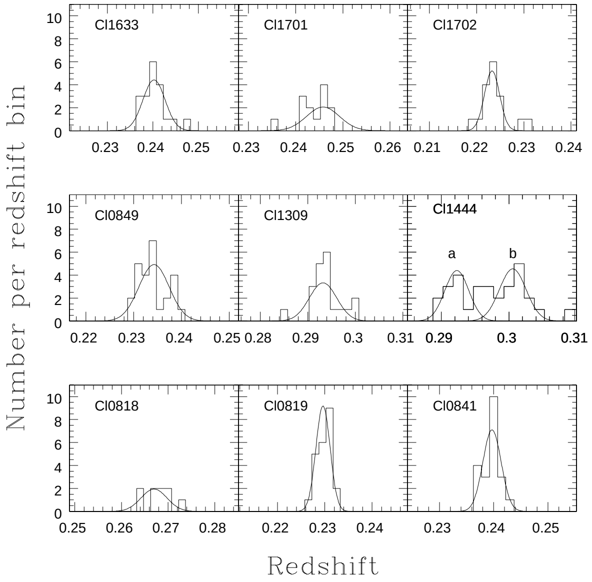

Figure 7. Redshift distributions for each of the clusters in our sample. The redshift range plotted represents 9000 km s^{-1} about the mean redshift, in the rest-frame of the cluster. The smooth curves overlayed are Gaussian functions with the computed centre and observed-frame velocity dispersion for each cluser. Note the dispersions tabulated in Table 1 are in the rest-frame of the cluster and include a small correction for the 100 km s^{-1} uncertainty on the redshifts.

2.7 The Catalogue

A catalogue of the relevant derived quantities for all cluster members (see definition in § 3.1) is given in Table 4. Galaxies are identified by an identification number from the photometric catalogue in column 1; serendipitous observations not in the original catalogue have an identification number of −99. The r magnitude, redshift and sky coordinates are given in columns 2–5. For galaxies observed with *HST*, column 6 lists the GIM2D B/T measurement. Note that the formal errors on B/T given by GIM2D are typically $\lesssim 0.02$; however these errors do not account for uncertainties in the sky level or point spread function, which likely dominate the measurement for faint galaxies. We have not, therefore, listed these uncertainties in Table 4. The spectral signal-to-noise ratio per resolution element is given in column 7, and the equivalent widths of $W_\circ$([OII]), $W_\circ(H\delta)$, and $W_\circ(H\alpha$+[NII]) are listed in columns 8-10.

In Figure 4 we show the images and spectra for all the cluster members with *HST* data. The brightest, central cluster members are shown separately in Figure 5, as are the sample of disk-dominated galaxies without emission lines (see § 4.1), which are shown in Figure 6. Note that the spectra in the vicinity of Hα are usually dominated by residuals from night-sky emission lines, not real features or Poisson noise. Also, the wavelength solution beyond $\lambda \sim 7000$ Å is occasionally inaccurate, resulting in a small misalignment with Hα. This has a negligible effect on our measurement, since the Hα line still always lies within the bandpass we use to measure the flux.

3 RESULTS

3.1 Dynamics

In Figure 7 we show the redshift histogram of each cluster. For most clusters, the median redshift and its dispersion were determined using the biweight estimator (Beers et al. 1990) on galaxies within $\Delta z = 0.02$ of the cluster. The exception is the double cluster Cl 1444, which has a bimodal redshift distribution, with a rest-frame velocity difference of 2080 km s^{-1}. In this case, the biweight estimator results in an unreasonably high dispersion for each peak in the distribution. Instead, we use a 2-sigma clipping method

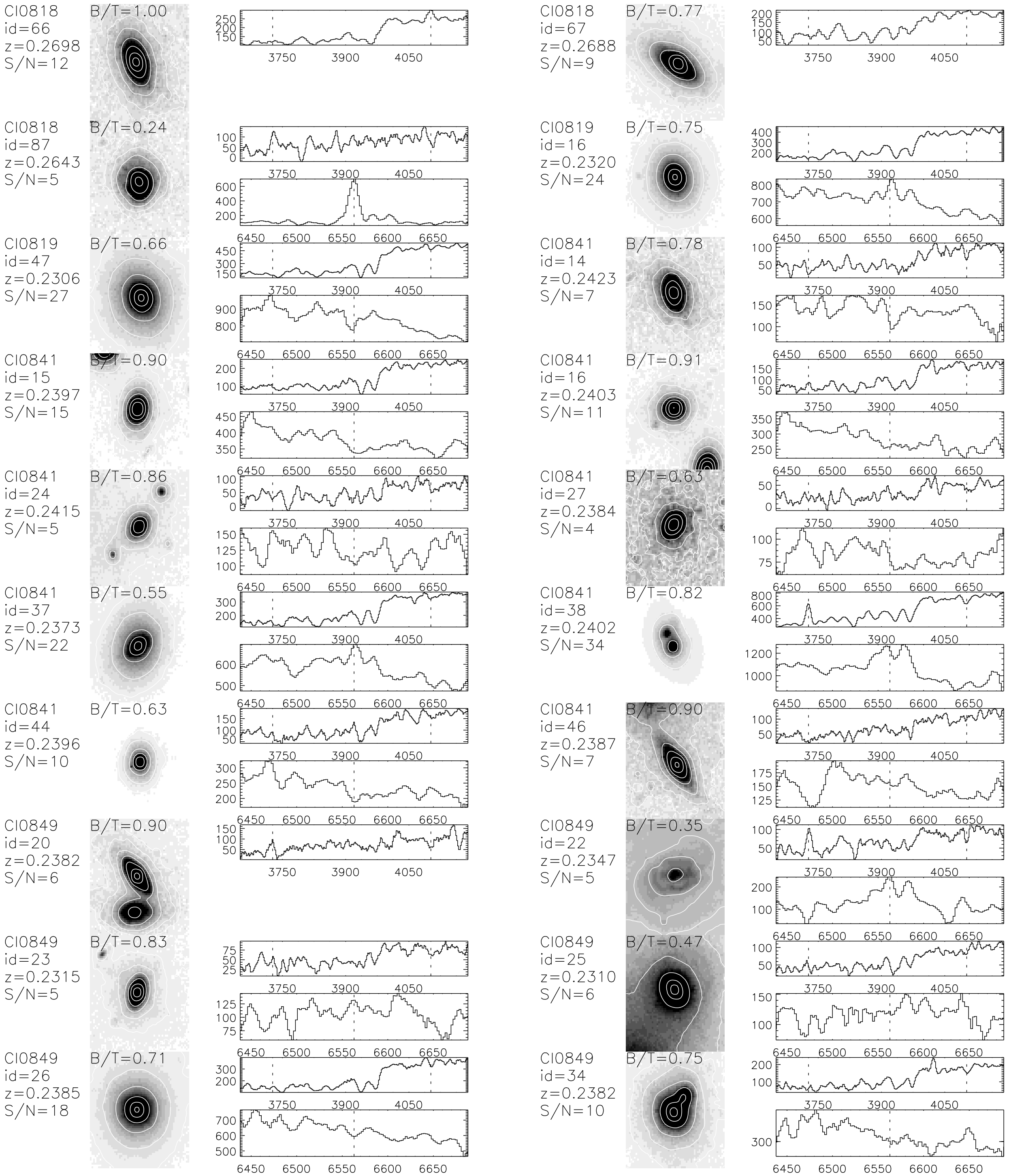

Figure 4. Images and spectra for all cluster members observed with *HST*. The F702W images are shown with logarithmically spaced contours over-plotted, and the B/T measurements from GIM2D are printed on the images. All images are $3'' \times 3''$, oriented north to the top and east to the left. To the left of the image, the galaxy identification and redshift are shown, together with the signal-to-noise ratio per resolution element of the spectrum, over $4050-4250$Å (rest frame). The spectra are smoothed to the instrumental resolution of ~ 15Å. For every galaxy we show the region around the [OII] and Hδ lines, with the location of those lines marked with a vertical, dotted line. When the spectrum near Hα is sufficiently clear of night-sky lines to permit a reasonable measurement of the Hα line strength, this region of the spectrum is also shown, with the position of Hα indicated. The y-axis of the spectra gives the number of CCD counts, after sky subtraction; the x-axis is the wavelength, in Å.

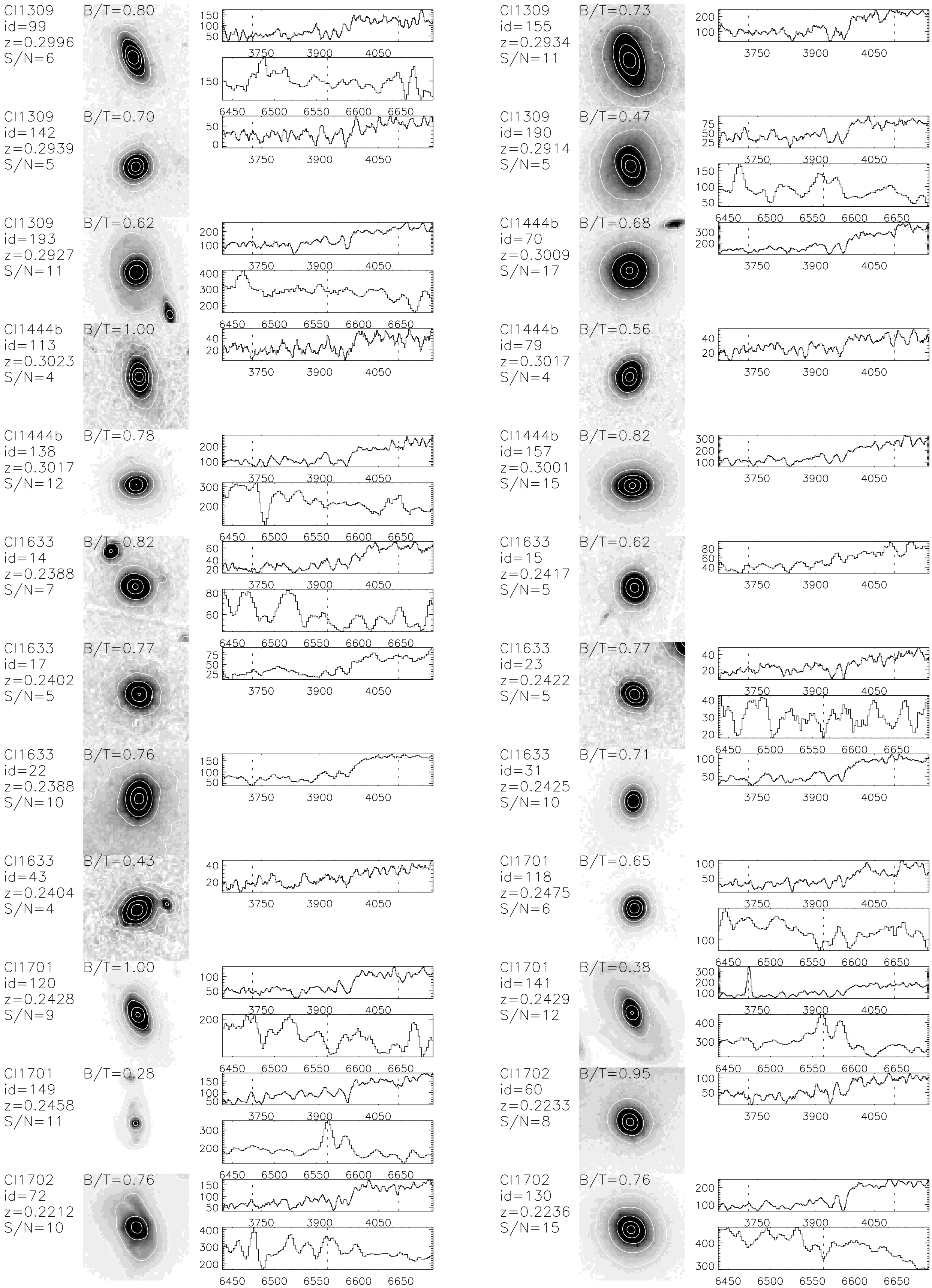

Figure 4. continued

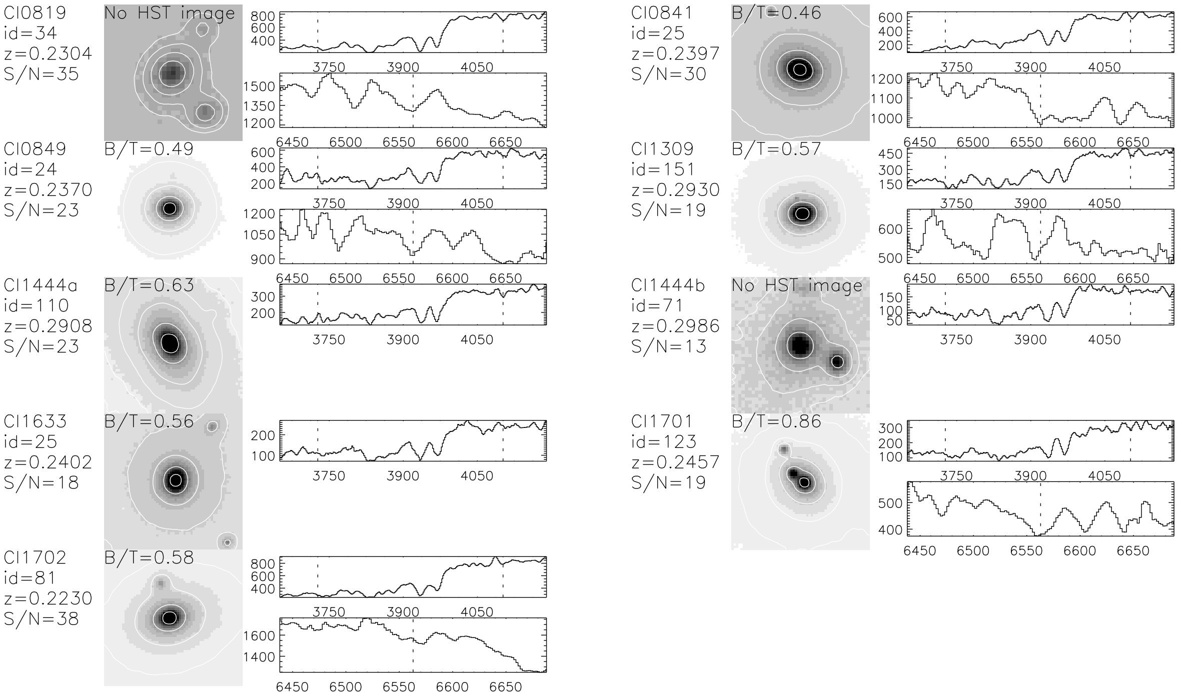

Figure 5. The central, bright galaxies of each of the clusters. The format of the figure is the same as for Figure 4. The central galaxy of Cl0818 lies behind a bright, foreground spiral which dominates the observed spectrum, and is not shown. Ground-based images are shown where *HST* images are not available; these are also 3″ on a side.

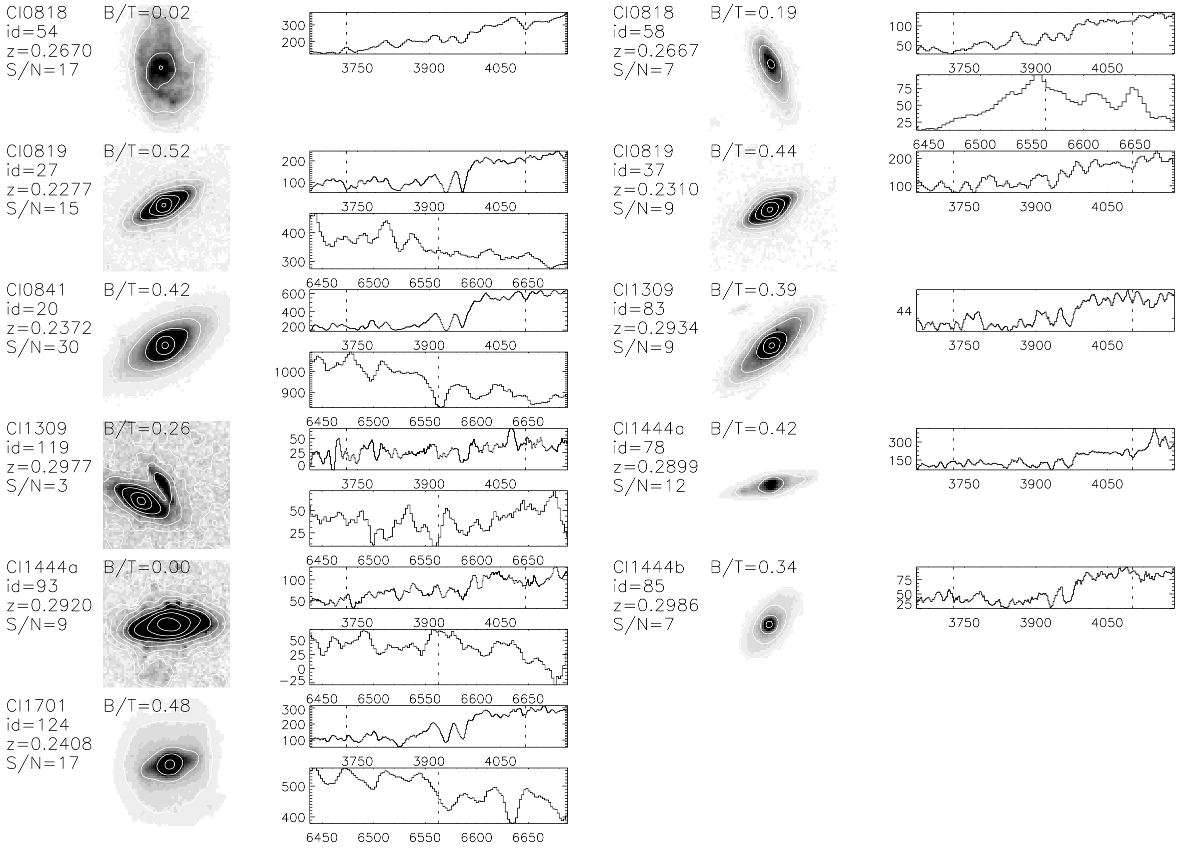

Figure 6. Disk-dominated galaxies without emission lines. The format of the figure is the same as for Figure 4.

to better characterise the distribution of each structure. We recognize this treatment as arbitrary, and do not consider the dispersions of these two clusters to be well determined. A small correction is made for the estimated uncertainty of 100 km s^{-1} on each redshift, by subtracting these in quadrature from the measured dispersion. For most of the clusters the velocity distribution includes ~ 20 galaxies, and is well fit by a Gaussian, shown as the smooth curves over-plotted in Figure 7. There appears to be a structure in redshift space between Cl 1701 and Cl 1702; with the small number of redshifts available, it is not possible to determine whether or not this substructure is associated with one of the clusters. The remaining clusters are well isolated from the surrounding field. Cluster members are taken to be all those within 3σ of the cluster velocity dispersion.

The velocity dispersion, its uncertainty, and the number of galaxies within 3σ of each cluster are listed in Table 1. The velocity dispersions of all the clusters are fairly similar, with a mean $\sigma = 548$ km s^{-1} and a standard deviation of 172 km s^{-1}. The uncertainty in velocity dispersion, determined by jackknife resampling, is generally quite large, > 200 km s^{-1}. In particular, it is much larger for the clusters Cl 1309, Cl 1701 and Cl 1702, which appear to have substructure in the wings of the distribution. We expect the virial radii to be R_v[Mpc]$\sim 0.0035(1+z)^{-1.5}\sigma$[km/s]$\sim 1.4$ Mpc (Girardi et al. 1998), or ~ 5.9 arcmin at $z = 0.25$. Because of the large uncertainties on the velocity dispersions, however, the virial radii of individual clusters are not well determined.

The measured velocity dispersions are in good agreement with those expected from the local correlation with X-ray luminosity, as shown in Figure 8. Here, the X-ray luminosities are estimated bolometric luminosities for a Universe with $\Lambda = 0.7, \Omega_m = 0.3, h = 0.7$, assuming gas temperatures of 3 keV. The $L_X - \sigma$ correlation is consistent with the local relation, over scales ranging from the richest clusters (David et al. 1993; Markevitch 1998) to groups (Xue & Wu 2000). It is now well known that this scaling is inconsistent with a purely self-similar model of the intracluster medium, but can be successfully matched by models with a substantial entropy floor due, perhaps, to the injection of energy from supernovae and AGN (Babul et al. 2002). However, our uncertainties on σ are too large to improve the existing constraints on the slope of this relation.

Figure 9 shows the normalised velocity-radius correlation for the ten clusters. The cluster centres are taken to be the position of the brightest galaxy (§ 3.2), which are always near the X-ray centres from Vikhlinin et al. (1998). The radius is the distance to this centre, normalised to the cluster virial radius, while the velocity is the velocity difference from the cluster mean, normalised to the 1-σ velocity dispersion. The cluster members are well-separated from the surrounding field. Emission line galaxies and disk-dominated galaxies both avoid the central regions of the cluster. However, there is no measurable difference between the dynamics of the emission line galaxies and the rest of the sample, as shown by the comparison of the normalised velocity histograms, in the right panel of Figure 9. Both velocity distributions are consistent with a Gaussian distribution of unity variance.

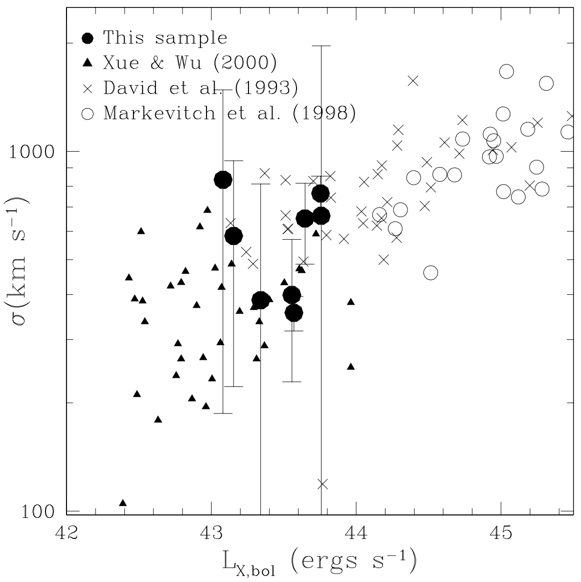

Figure 8. The correlation between velocity dispersion σ and bolometric X-ray luminosity ($\Lambda = 0.7, \Omega_m = 0.3, h = 0.7$) for our sample is shown as *solid circles* with 1$-\sigma$ error bars on the velocity dispersion. This is compared with three local cluster samples, as indicated; error bars are omitted on these points for clarity.

3.2 Brightest Cluster Galaxies

The central galaxies of each cluster are shown in Figure 5. The central galaxy of Cl0818 lies directly behind a bright, foreground spiral galaxy. The spectrum shows features from both galaxies, but is dominated by the foreground galaxy so is omitted from the rest of the analysis. All the other central galaxies are giant elliptical galaxies, none of which show emission lines, nor the prominent Balmer absorption lines that would indicate the presence of recent star formation activity. Star formation in central galaxies (e.g. see Crawford et al. 1999) is likely to be associated with cooling flow activity, which is now known to produce a reservoir of cold molecular gas (Edge 2001). Because only extended sources are included in the catalogue of Vikhlinin et al. (1998), at the faint flux limit the catalogue is biased against clusters with strong cooling flows (if they even exist at these low luminosities), which may therefore be related to the lack of emission in the central galaxies.

3.3 Spectral properties

The cumulative distribution of $W_\circ$([OII]) for the 167 cluster galaxies, weighted by the spectroscopic selection function, is shown in Figure 10. This sample is shown limited to $M_r \leq -18.5 + 5\log h$, corresponding to $R \sim 20$ at $z = 0.25$, to allow a fair comparison with the field and cluster samples of Balogh et al. (1997, see § 4). The mean (weighted by the selection function) is $W_\circ$([OII])$=$ 3.2Å, and the median is $W_\circ$([OII])$=$ 0.7Å. A total of 36 galaxies have $W_\circ$([OII])$>$ 5Å; accounting for the spectroscopic selection function, this corresponds to $\sim 22\%$. None of the galaxies have $W_\circ$([OII])$>$ 45Å, or otherwise have spectra characteristic of a strong starburst.

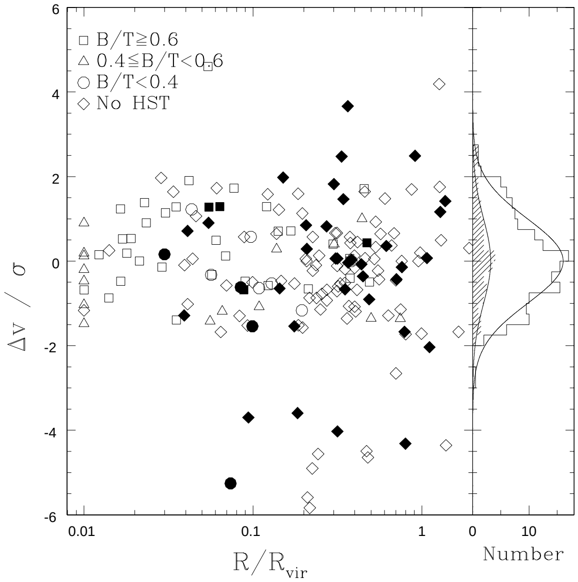

Figure 9. The normalised velocity-radius relation for galaxies in the ten clusters. The velocities are measured relative to the cluster redshift, normalised to the cluster velocity dispersion. The radii are measured from the position of the central, bright galaxy (shown at $R/R_{\rm vir} = 0.01$ for display purposes), and normalised to the cluster virial radius. *Filled symbols* represent galaxies with $W_\circ$([OII])> 5Å. Only galaxies within 6 times the cluster velocity dispersion σ are shown; cluster members are selected to be those within 3σ. The symbol shape corresponds to the galaxy morphology, as indicated in the legend. The normalised velocity distribution for cluster members is shown in the right-hand panel, for the full sample *(open histogram)* and the emission line galaxies ($W_\circ$([OII])> 5Å, *filled histogram*). Both are consistent with a Gaussian distribution of unit variance, shown as the smooth, solid curves.

The fraction of emission-line galaxies, therefore, is comparable to the fraction of disk-dominated galaxies at our spectroscopic magnitude limit (see § 2.6). In Figure 11 we show these fractions as a function of luminosity. The emission line fraction increases strongly with decreasing luminosity, which is a well-known result (e.g. Ellis et al. 1996; Lin et al. 1996; Lewis et al. 1999; Christlein 2000; Balogh et al. 2001). This trend is also seen, with less significance, in the fraction of disk-dominated galaxies, though the *HST* sample is smaller and morphologies are not measured for the faintest galaxies. The two fractions are comparable at all luminosities. However, the excess of disk galaxies relative to emission line galaxies around L^*, although statistically insignificant, corresponds to a bona-fide population of "anemic" disk galaxies, which we discuss in § 4.1.

In Figure 12 we show the dependence of emission line equivalent width on B/T. Only two bulge-dominated galaxies ($B/T > 0.6$) show $W_\circ$([OII])> 5Å. One of these (Cl0841#38) is a double-nucleated galaxy with strong, broad [NII] indicative of an active galactic nucleus (AGN). The other, Cl0849#20 is an Sa galaxy with a clear disk component, close to another bright galaxy which complicates the surface-brightness fitting procedure. Similarly, of the eight disk-dominated galaxies with $B/T < 0.4$, only three have $W_\circ$([OII])> 5Å, and one of these has broad Hα and

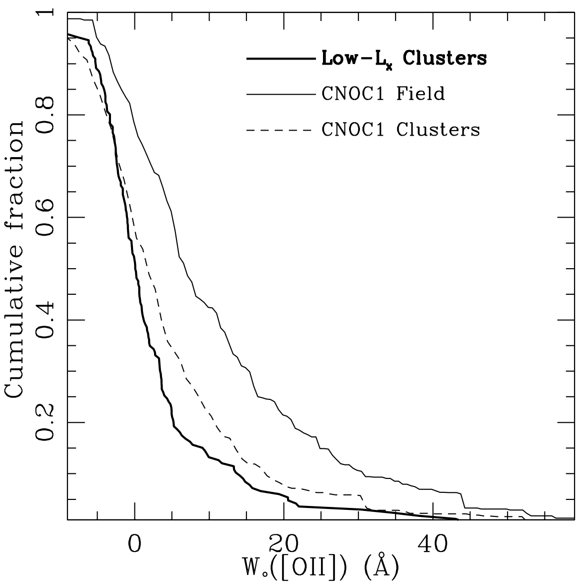

Figure 10. The cumulative distribution of $W_\circ$([OII]), for the 167 cluster members with reliable measurements, brighter than $M_R \sim -18.5 + 5\log h$. The distribution is weighted by the spectroscopic selection function. This is compared with the distribution in the field and in clusters of high X-ray luminosity at $z \sim 0.3$, from Balogh et al. (1997). Both our survey and that of Balogh et al. sample the clusters out to the virial radius, and are statistically complete at this luminosity.

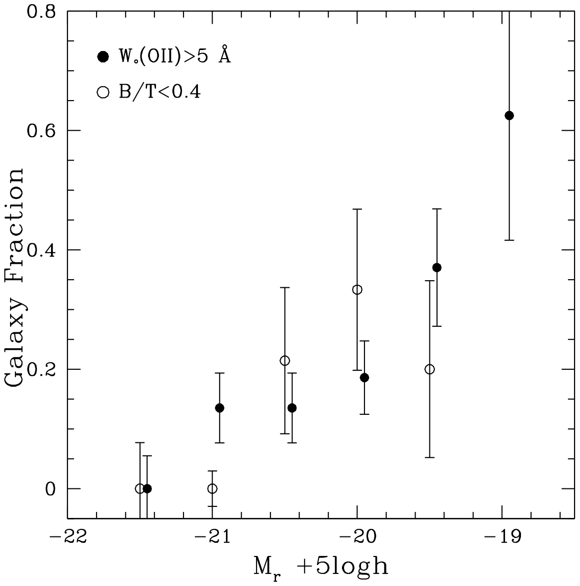

Figure 11. The fraction of emission-line galaxies ($W_\circ$([OII])> 5Å, *solid circles*) and disk-dominated galaxies ($B/T < 0.4$, *open circles*) as a function of galaxy luminosity. Only bins with at least three galaxies are shown. Error bars are jackknife estimates or, in the case where the fraction is zero, estimates assuming Poisson statistics.

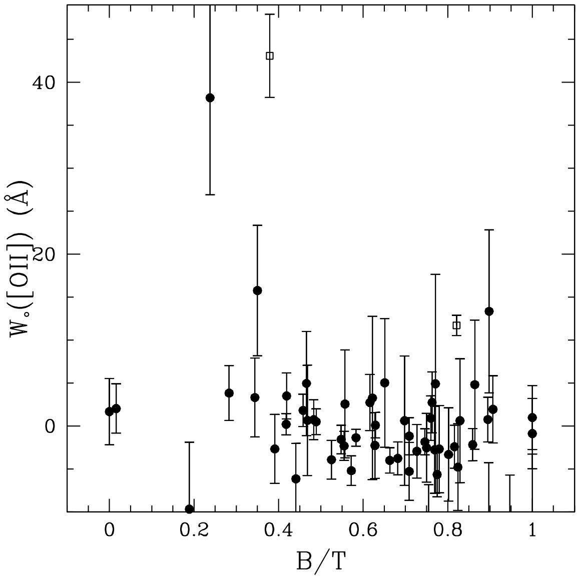

Figure 12. The equivalent width of [OII] as a function of fractional bulge luminosity, B/T. The two galaxies represented by *open squares* have strong, broad [NII] emission characteristic of non-thermal emission.

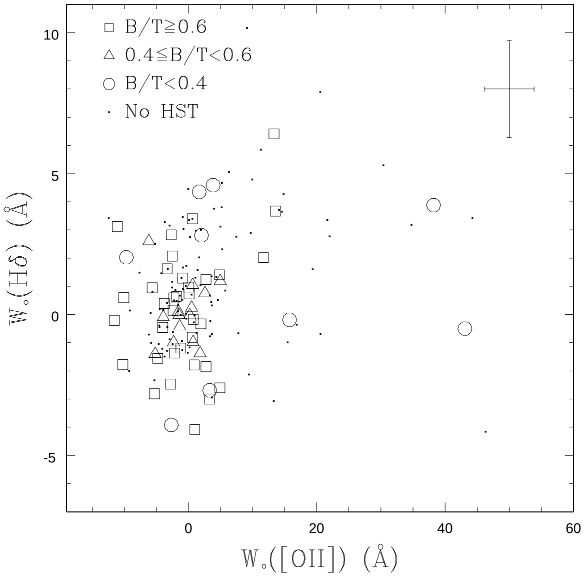

Figure 13. The rest frame equivalent width of Hδ is shown as a function of $W_\circ$([OII]), for all cluster members in which both lines could be measured. For galaxies with *HST* imaging, the symbols correspond to the B/T ratio, as indicated in the legend. The sample error bars show the median $1-\sigma$ uncertainty in each index.

strong [NII] emission indicative of an AGN. This fraction of emission-line disk galaxies is consistent with the values seen in the inner regions ($< 0.1R_{\rm vir}$) of the high X-ray luminosity CNOC1 clusters (Balogh et al. 1998), and Abell 1689 at $z = 0.18$ (Balogh et al. 2002a). All of these galaxies have luminosities within ~ 0.5 mag of $M_r^* \sim -20.3 + 5\log h$.

While the [OII] line is present where star-formation is ongoing, the Hδ absorption line is expected to be strong in galaxies in which star formation has occurred sometime within the last $\sim$ 500 Myr or so (e.g. Couch & Sharples 1987; Poggianti et al. 1999; Balogh et al. 1999; Poggianti & Wu 2000). Measurements of $W_\circ(H\delta)$ are shown as a function of $W_\circ$([OII]) in Figure 13. A population of galaxies with strong Hδ but no detectable emission are strikingly absent from this sample. Using the spectral classifications of Dressler et al. (1999), a k+a galaxy is one with $W_\circ(H\delta)>$ 3Å and no detectable emission. This definition is somewhat arbitrary, and any physical interpretation of the Hδ strength needs to account for differences in the way in which the line is measured. Although fourteen of the galaxies in our sample formally satisfy Dressler et al.'s definition of a k+a galaxy, most of these have $W_\circ(H\delta)$ very close to the limit of 3Å (Figure 13). Given the large uncertainties (systematic and random) in the measurements and the model-sensitivity of the interpretation, we cannot claim that the spectral properties of this population are strikingly unusual (see § 4.1 for more discussion). We are only able to identify four galaxies which show $W_\circ(H\delta)>$ 4Å with at least 1σ confidence. All of these galaxies show nebular emission, and thus are e(a) galaxies in the classification scheme of Dressler et al. (1999). Both of these populations will be discussed further in § 4.1.

3.4 Population Gradients

In Figure 14 we show $W_\circ$([OII]) as a function of cluster-centric radius. The cluster centres are taken to be the position of the brightest galaxy. There is little trend in the mean or median equivalent width of the sample; both are always $\lesssim$ 5Å out to $1h^{-1}$ Mpc. Galaxies with strong emission lines are only found outside the cores of these clusters, beyond $\sim 0.05h^{-1}$ Mpc, and the fraction of galaxies with $W_\circ$([OII])$>$ 5Å increases from $<$ 10% within this radius to $\sim$ 30% at $1h^{-1}$ Mpc, approximately the virial radius estimated for these systems. However, this may just be due to the fact that there are fewer galaxies in the core so the wings of the highly skewed distribution are insufficiently sampled. A Kolmogorov-Smirnov test cannot reject the hypothesis that the $W_\circ$([OII]) distributions within and beyond $0.1h^{-1}$ Mpc are drawn from the same population.

Galaxy morphologies are known to correlate strongly with the local density of galaxies (Dressler 1980; Postman & Geller 1984; Domínguez et al. 2001). More recently, a similar density-dependence has been found for the average star formation rate of galaxies (Couch et al. 2001; Kodama et al. 2001; Pimbblet et al. 2002; Lewis et al. 2002; Gomez et al. 2002). To compute the local, projected galaxy density, we measure the area enclosing the fifth nearest neighbour to each cluster member. We do this using the full photometric catalogue (i.e., not just galaxies with redshifts) and statistically correct for the average background density. This is similar to the definition of Dressler (1980), but we use the fifth nearest neighbour rather than the tenth because we found the latter method tends to wash out the densest regions of the clusters. Our results are unchanged if we adopt the tenth nearest-neighbour definition, but the resolution of the dense cores is poorer. It is important to compute the

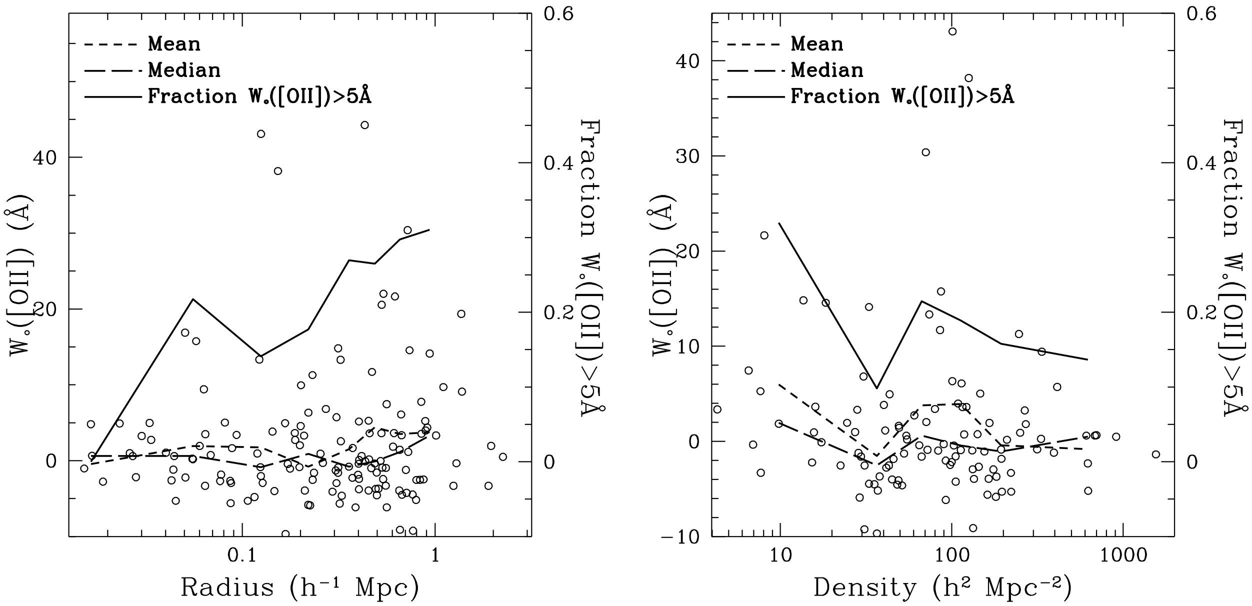

Figure 14. Left: [OII] emission line strengths as a function of cluster-centric distance. The *long-dashed* and *short-dashed* lines show the median and mean value, respectively, in bins of varying width, each containing 20 points. The *solid* line represents the fraction of galaxies with $W_\circ$([OII])> 5Å, according to the scale on the right side of the figure. These quantities are weighted by the spectroscopic selection function, for a sample with $R < 20.5$. **Right:** The same as the left panel, but as a function of local projected density. The density is computed from the distance to the fifth nearest-neighbour, and corrected for the background using the number counts of Lin et al. (1999).

density to a fixed luminosity limit in all clusters, and we adopt $M^* + 1.5$, which corresponds to $M_r \sim -19.5 + 5\log h$, or $R = 20$ at $z = 0.25$. This limit is consistent with that of Dressler (1980), and is 3 mag brighter than that used in Paper I. We do not include the double cluster Cl 1444 in this analysis, because the projected surface density cannot be reliably determined from the photometric properties alone. For the background correction, we use the field number counts in R_c of Lin et al. (1999). The number of galaxies brighter than $R_c = 20$ is 1460±40 per square degree, where the error does not include cosmic variance. This is adjusted as necessary for the magnitude limit of each cluster. Finally, we invert the area containing the fifth nearest neighbour to obtain the density in units of galaxies per Mpc^2.

In the right panel of Figure 14 we show the $W_\circ$([OII]) as a function of local projected galaxy density. In the very densest regions, $\Sigma > 500\mathrm{h}^2\mathrm{Mpc}^{-2}$, there are no galaxies with strong emission lines. However, below this limit there is no evidence for a trend with density. The fraction of galaxies with $W_\circ$([OII])> 5Å remains $\lesssim$ 20%, and the median is < 5Å.

The lack of a correlation of $W_\circ$([OII]) with density is surprising, especially given the local result of Lewis et al. (2002), that the correlation holds in all clusters, independent of mass. This is possibly a consequence of our small sample size, since there are very few galaxies with emission lines in the full sample. In particular, in the lowest density regions we have very few galaxies (13 with $\Sigma < 20$), and thus cannot precisely determine the fraction of emission line galaxies, especially when that fraction is $\ll 1$.

4 DISCUSSION

4.1 Anemic spirals, starburst and post-starburst galaxies

Despite the similarity in the fraction of disk-dominated and emission-line galaxies ($\sim$ 20%), there is a significant population of disk-dominated galaxies in our sample that do not have detected emission lines. This may be analogous to the population seen in more massive clusters (Poggianti et al. 1999), and is a very cluster-specific population; in local field samples, almost all disk galaxies show strong emission lines (Kennicutt 1983; Jansen et al. 2000). In Figure 12 we showed that there were six galaxies in our sample with $B/T < 0.4$ and $W_\circ$([OII])< 5Å. In one of these galaxies, Cl 1701#149, there is Hα emission, $W_\circ(H\alpha$+[NII])= 23±3Å, which is weak enough to be consistent with the low observed $W_\circ$([OII]). The remaining five galaxies are all convincing disk galaxies with no detectable emission. If we relax our definition of a disk-dominated galaxy to include those with larger B/T ratios ($B/T < 0.5$), we find five other clear examples of galaxies with a disklike morphology but no evidence of nebular emission. We also include a galaxy (Cl 1309#119) without Hα emission ([OII] is undetermined) to bring the total sample of such galaxies to eleven. This population therefore comprises 6.5 ± 2% of the cluster members, and 57 ± 17 % of the disk-dominated ($B/T < 0.5$) population. These are consistent with the fractions of late-type (later than Sa) galaxies without emission found in the z$\sim$ 0.4 cluster sample of Poggianti et al. (1999). The images and spectra of these galaxies in our clusters are shown in Figure 6. Most appear to be early or mid-type spirals, but have very smooth disks, without strong spiral structure or prominent HII regions, and thus

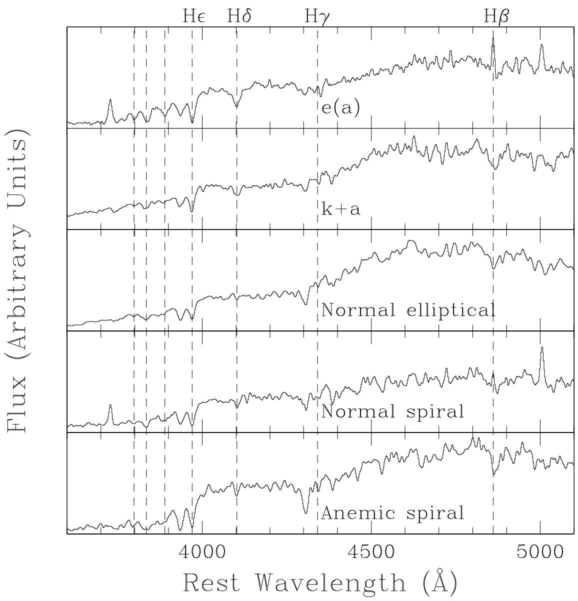

Figure 15. Coadded spectra of 11 anemic spiral galaxies ($B/T < 0.5$ and no emission lines), 13 normal spiral galaxies, 34 elliptical galaxies ($B/T > 0.6$), 14 k+a galaxies ($W_\circ(H\delta)>$ 3Å and $W_\circ$([OII])$<$ 5Å), and 8 e(a) galaxies. The spectra are renormalised to template continuua from Kinney et al. (1996) as described in the text, and smoothed to the instrumental resolution of ∼ 15Å. The positions of the Balmer absorption lines are marked with *dashed*, vertical lines.

resemble anemic galaxies (van den Bergh 1976, 1991). Particularly interesting is Cl0818#58, a smooth spiral galaxy that is elongated and asymmetric, and has the appearance expected of a galaxy in the process of being stripped (Quilis et al. 2000). We note that the slit width is 1.5″, half the width of the postage-stamp images shown in Figure 6 and comparable to the size of the galaxies; therefore we do not expect the lack of emission to be due to an aperture bias.

To improve upon the signal-to-noise ratio of individual spectra, we have coadded four classes of spectra, in Figure 15. In particular, we show the coadded spectra of the anemic spiral sample, including all galaxies with $B/T < 0.5$ and no detectable emission lines. Before coadding, the individual spectra are shifted to zero redshift and the shape of the continuum in the range 3500–5100Å is removed with a spline fit. The spectra are then averaged pixel by pixel, weighted by the median flux in the rest-frame wavelength range 4050–4250Å, to give more weight to better quality data. For presentation purposes, we fit the continuum of the Sb template spectrum from Kinney et al. (1996), and rescale our spectra to this continuum. Finally, the spectra are smoothed to the instrumental resolution of ∼ 15 Å.

The coadded anemic spiral spectrum can be directly compared with the coadded spectra of thirteen normal spiral galaxies (disk galaxies with emission lines, including clear examples of spiral galaxies in the absence of *HST* imaging) and 34 early-type galaxies (with *HST* imaging and $B/T > 0.6$), also shown in Figure 15. The early-type galaxies are renormalised to the continuum of the elliptical template of Kinney et al. (1996). Apart from the lack of emission lines, the anemic spiral spectra look quite similar to those of the normal spiral galaxies. In particular, the Balmer series is stronger than seen in the early-type spectra, comparable to that of normal spirals ($W_\circ(H\delta)\sim$ 2.5Å). On the other hand, some absorption lines in the anemic galaxies, most notably the G-band at ∼ 4300Å, are more similar to the strengths seen in elliptical galaxies.

It is remarkable that none of the galaxies in our sample show the very strong emission lines characteristic of a strong starburst. The strongest emission-line galaxies are almost all normal spiral galaxies (with the exception of the merging/interacting galaxies Cl0841#38 and Cl0849#20), and the fraction of strong emission-line galaxies is small relative to the fraction observed in the field at this redshift. Furthermore, as shown in § 3.3, we find no convincing examples of the Balmer-strong galaxies without emission lines which may be in a post-starburst phase (e.g. Couch & Sharples 1987; Dressler & Gunn 1983; Balogh et al. 1999; Poggianti et al. 1999). Formally, there are fourteen galaxies which are classified k+a according to Dressler et al. (1999), though all but three of these have $W_\circ(H\delta)\sim$ 3Å, close to the arbitrarily-defined cutoff strength. The coadded spectrum of these galaxies is shown in Figure 15. No evidence for Hβ or [OIII]λ5007 emission is seen, confirming that the lack of [OII] emission is real. Most of the spectrum appears similar to that of the elliptical population although, by selection, the Hδ absorption line is relatively strong. Most notably, the other Balmer lines are not especially prominent, which suggests that many of the high Hδ measurements are cases where the substantial measurement uncertainty results in an overestimate of the line strength, as suggested by Balogh et al. (1999). We do find eight galaxies with $W_\circ(H\delta)>$ 4Å, though the errors are such that only four of these exceed 4 Å with $> 1\sigma$ confidence. All of these galaxies have emission lines, and are thus e(a) galaxies (Poggianti et al. 1999). The coadded spectrum of these eight galaxies is also shown in Figure 15. The Balmer series is clear even blueward of Hϵ, and is enhanced relative to that seen in the normal spiral, anemic spiral, or k+a population. Emission lines at Hβ and [OIII]λ5007 are seen, in addition to [OII].

The rarity of galaxies with strong Balmer absorption lines is in good agreement with the results seen in X-ray luminous clusters at $z\sim 0.3$, from the work of Balogh et al. (1999). The discrepancy with the relatively high fraction of Hδ-strong galaxies in clusters at $z\sim 0.4$ (Poggianti et al. 1999) is still not understood. One suggestion that has been put forward is that the clusters of Poggianti et al. are dynamically younger, with more galaxy-galaxy interactions than in the more relaxed CNOC1 clusters (Balogh et al. 1999). However, we expect such interactions to be even more important in our sample of clusters, due to their low velocity dispersions, and yet no large population of starburst or post-starburst galaxies is found. The fact that these clusters are X-ray selected and have central, giant elliptical galaxies, may suggest that they are dynamically old systems, in which all merger-induced star formation activity took place several Gyr ago. However, we still cannot rule out the possibility that the difference is due in part to evolution between $z\sim 0.25$ and $z\sim 0.4$ (corresponding to a difference of 1.3 Gyr in our assumed cosmology), or to spectroscopic sample selection effects, as discussed in Balogh et al. (1999).

4.2 Comparison with X-ray luminous clusters

The ten clusters analysed in this work are analogous to more massive clusters in several ways. Dynamically, they appear to be relaxed systems in which the X-ray centre coincides closely with the position of the giant elliptical galaxy. Interestingly, none of these central galaxies show any sign of star formation. In contrast, in the *ROSAT* Brightest Cluster sample of clusters, $\sim 27\%$ have central galaxies which show emission lines, approximately independent of X-ray luminosity (Crawford et al. 1999). The clusters in our sample have luminosities which place them all in the lowest-luminosity bin of Crawford et al.'s figure 4, where $\sim 22 \pm 10\%$ have central galaxies with Hα emission. Thus, our results for a sample of nine clusters (omitting Cl0818, for which no spectrum of the central galaxy was obtained) are not strongly inconsistent with this fraction.

In massive clusters, Carlberg et al. (1997) found that the velocity dispersion of blue galaxies is $\sim 30\%$ larger than that of the red galaxies, and suggested this was a sign that the star-forming galaxies are not yet in virial equilibrium with the cluster potential. A similar conclusion was reached by Dressler et al. (1999), who found that recently star-forming galaxies have a velocity dispersion $\sim 40\%$ larger than that of the passive, elliptical population. We find no statistically significant difference in the dynamics of the emission-line galaxy population, relative to that of the whole population. However, our sample of emission line galaxies is too small to claim a significant difference from the more massive clusters. Using a Kolmogorov-Smirnov test, we can only rule out, at the 99% or greater confidence level, velocity distributions (for the emission-line population) that are more than 2.8 times broader than the cluster velocity dispersion.

The distribution of $W_\circ([\text{O}\textsc{ii}])$ in our cluster sample (Figure 10) is similar to that of Balogh et al. (1997), measured, to the same luminosity limit, for the CNOC1 sample of X-ray luminous clusters at $z \sim 0.3$ (Yee et al. 1996; Carlberg et al. 1996). Both our sample and the high X-ray luminosity clusters show $W_\circ([\text{O}\textsc{ii}])$ distributions that are greatly suppressed relative to the field near that redshift, also taken from Balogh et al. (1997). Note that, since it is generally easier to get redshifts for emission line galaxies, any incompleteness in our sample for this reason is likely to lead to our overestimation of the number of emission line galaxies in our sample, thus strengthening our conclusions. Therefore, we conclude that over ~ 2 orders of magnitude in cluster X-ray luminosity, there is little difference in the mean age of the stellar population for galaxies more luminous than $\sim M^* + 2.5$. It must, therefore, be a local process, rather than a global one associated with the large-scale mass distribution, which affects the star formation rates of galaxies.

Both the present study and the CNOC1 cluster sample present data out to approximately the virial radius of the clusters. However, the CNOC1 clusters are more massive, and there may be a difference in the range of local densities sampled. To test this, we have evaluated the local density for every galaxy in the CNOC1 sample, using the same method, and the same luminosity limit, as for our Low–L_X cluster sample. In Figure 16 we show the fraction of galaxies with $W_\circ([\text{O}\textsc{ii}]) > 5$Å as a function of local density, for the present sample and that of Balogh et al. (1997). The two functions are indistinguishable within the uncertainties, and thus we conclude that the level of star formation in the Low–L_X clusters is comparable to that in the CNOC1 clusters at all densities probed. In particular, we see little trend with local density, and the fraction of emission-line galaxies is always $< 30\%$.

In Paper I we showed that the Low–L_X clusters have a significantly larger fraction of disk-dominated galaxies brighter than $R \sim 23$ than more massive clusters (Paper I). In particular, the data showed that, at a given local density, the bulges in massive clusters are systematically more luminous than the bulges in the Low–L_X clusters, while the disk luminosity function is independent of cluster mass. In the present work we do not find a large difference between the fraction of emission-line galaxies at $R < 20$. This may suggest that galaxy morphology (in particular, bulge size) is partially sensitive to large-scale structure, while star formation properties are not. Alternatively, this may just be reflecting the difference in the luminosity ranges considered in the two studies; unfortunately, the *HST* sample is too small to determine the disk fraction at $R < 20$ with enough precision to determine whether or not the small difference found in Paper I holds at this brighter magnitude.

Very recently, analysis of the correlation between star formation rate and local projected density in nearby clusters from the 2dF galaxy redshift survey (Lewis et al. 2002) and the Sloan Digital Sky Survey (Gomez et al. 2002) has shown that star formation is reduced below the global average in all environments where the local density exceeds ~ 1 galaxy (brighter than $M^* + 1$) per Mpc^2. This was shown to hold in systems of low velocity dispersion, and well outside the virialised cluster regions. Although our sample does not extend to such low densities, we confirm that, even at $z \sim 0.25$, where the Butcher-Oemler effect (Butcher & Oemler 1984; Ellingson et al. 2001) is beginning to appear, dense regions in low-mass structures have very low star formation rates[5]. It will be of enormous interest to trace the star-formation rate correlation with density out to comparably low densities at this redshift and beyond, to compare with the low redshift data.

4.3 Comparison with the morphology-density relation

It is interesting to compare the $W_\circ([\text{O}\textsc{ii}])$ dependence (or lack-thereof) on density with the morphology-density relation (Dressler 1980). We show the measured disk fraction for our sample in this region as the heavy, dashed line in Figure 16. Since our *HST* imaging is restricted to the central regions of the clusters, reliable morphologies are only available for the densest regions. To make a comparison at lower densities, we show the fraction of spiral and irregular galaxies in the sample of Dressler (1980), as a function of local density, converted to $h = 1$ for consistency with the results shown here. At the high density end, Dressler's data

---

[5] Deriving a star formation rate from the $W_\circ([\text{O}\textsc{ii}])$ requires knowledge of the galaxy $B-$band luminosity, metallicity and dust content. If these quantities in our clusters are similar to those in the $z = 0$ clusters, than the similarity in $W_\circ([\text{O}\textsc{ii}])$ distributions corresponds to a similarity in star formation rate distributions.

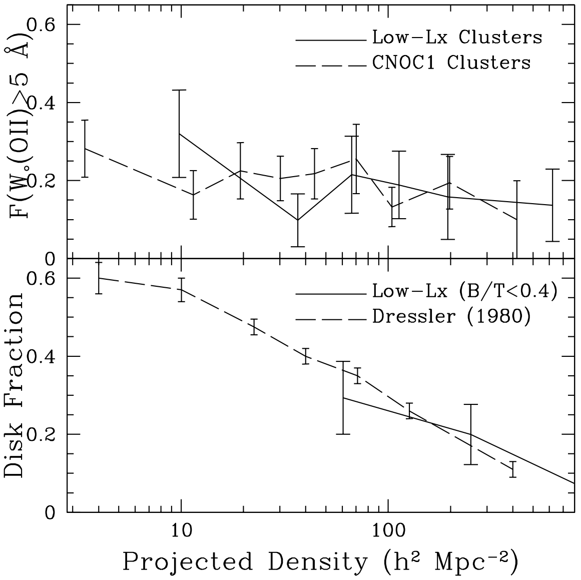

Figure 16. Top: The fraction of galaxies with $W_\circ$([OII])> 5 Å in the present sample (*solid line*) and in the CNOC1 sample (Balogh et al. 1997), as a function of local, projected galaxy density. Error bars are 1-σ jackknife estimates. The fractions corresponding to the present sample are computed in equally populated bins containing 20 galaxies. The CNOC1 data are presented in bins each with 40 galaxies. **Bottom:** The fraction of disk galaxies ($B/T < 0.4$) from our *HST* sample as a function of local density (*solid line*) is compared with the fraction of spiral and irregular galaxies from Dressler (1980, *dashed line).*

are consistent with the disk fractions we measure from the *HST* data.

There is a much stronger trend compared with the $W_\circ$([OII]) data, and the fraction of spiral galaxies increases to ∼ 60% at the lowest densities probed by our spectroscopic sample. At densities $\lesssim 50$ Mpc^{-2}, the fraction of spiral galaxies expected from Dressler's data is at least a factor of two larger than the fraction of galaxies with $W_\circ$([OII])> 5Å, significant at the $> 2\sigma$ level. In agreement with the results of Balogh et al. (1998), Couch et al. (2001) and Lewis et al. (2002), this suggests that the morphology-density relation is at least partially independent of the star-formation rate dependence on density.

4.4 Physical mechanisms

We can use these results to draw some conclusions about the physical mechanisms which may be responsible for the low star formation rates among galaxies in dense environments. The clusters in this sample have velocity dispersions which are typically a factor ∼ 2 less than those of the most massive clusters in the universe at $z \sim 0.25$. Since the ram-pressure force on a galaxy travelling through the intracluster medium is proportional to v^2 (Gunn & Gott 1972), we expect ram-pressure stripping of disk gas to be ∼ 4 times less effective in our cluster sample than in more massive clusters. In particular, models suggest that ram-pressure effects should be negligible in clusters with virial temperatures $kT \sim 2$ keV (Fujita & Nagashima 1999), corresponding approximately to the expected temperatures of our Low–L_X cluster sample. However, this difference is not reflected in the current star formation rates of the observed galaxy population. Therefore, we conclude that ram-pressure stripping within clusters is not primarily responsible for the low star formation rates. This is in good agreement with the results of other studies, which have shown little or no trend in blue galaxy fraction with cluster X-ray luminosity (Fairley et al. 2002; Pimbblet et al. 2002).

Secondly, we have not found a population of starburst galaxies, nor evidence for a large population of galaxies which have had a recent burst. This is in agreement with more complete Hα studies of more massive clusters at $z \sim 0.3$ (Couch et al. 2001; Balogh et al. 2002a). Thus, starbursts induced by the cluster environment (whether by interactions with the intracluster gas or with other galaxies) do not appear to be an important process, at least at the epoch at which the clusters are observed. There remain two appealing scenarios which are consistent with our data. The population gradients observed in rich clusters are consistent with models of "strangulation", in which satellite galaxies in haloes of any mass are stripped of their hot gas and consequently consume their available fuel supply fairly gradually (Larson et al. 1980; Balogh et al. 2000; Diaferio et al. 2001; Okamoto & Nagashima 2001; Bekki et al. 2002). The appearance of the disk-dominated galaxies which show no sign of star formation (Figure 6) seems to support this hypothesis. With the possible exceptions of Cl0818 #58, which has a highly asymmetric appearance one might expect of a galaxy interacting strongly with the ICM, and Cl 1309#119, which may be interacting with a larger galaxy, all of these galaxies are fairly isolated, spiral galaxies with smooth disks and no sign of strong disturbance or bright HII regions. The other possibility is that the galaxy transformation occurs in even smaller systems — galaxy groups — in the cluster infall region (Zabludoff & Mulchaey 1998; Kodama et al. 2001). In particular, at higher redshift galaxy groups are denser systems, with larger velocity dispersions than their local counterparts, and even processes like ram-pressure stripping may be able to take place (Fujita 2001). Furthermore, this may be the environment in which "strangulation" itself is most effective, and subsequent evolution within clusters may make little difference to the observable properties of the population (Okamoto & Nagashima 2001). The next step is therefore to focus on galaxy groups at a series of redshifts; in particular, galaxies in environments close to the "critical density", at which environmental effects first become observable (Kodama et al. 2001; Lewis et al. 2002; Gomez et al. 2002).

5 CONCLUSIONS

We have analysed ground-based spectroscopy and *HST*-based morphologies of galaxies in ten clusters at $z \approx 0.25$ with low X-ray luminosities. The sample includes 165 galaxies brighter than $R = 20.5$, which corresponds to $M_r = -19 + 5\log h$ at $z = 0.25$. We have measured morphologies using the GIM2D surface-brightness fitting software of Simard et al. (2002), and the strengths of important spectral features, in particular the [OII] emission line. The properties of the ten clusters can be summarized as:

- All ten clusters host a giant elliptical galaxy near the centre of the X-ray emission. None of the nine central galaxies for which we have a reliable spectrum show emission lines.

- Apart from the double cluster Cl 1444, and the close pair of clusters Cl 1701 and Cl 1702, all cluster velocity dispersions are consistent with a single Gaussian, and they appear dynamically well-separated from the surrounding field. Thus, they appear to be evolved systems in approximate dynamical equilibrium.
- The measured velocity dispersions range from $\sim$ 350–850 km s^{-1}, and are consistent with the local $L_X - \sigma$ relation observed in larger samples (e.g. Xue & Wu 2000).
- The fraction of cluster galaxies with $W_\circ$([OII]) > 5Å (2σ confidence limit) is 22±4%. The mean is $W_\circ$([OII])= 3.2Å, and the median is $W_\circ$([OII])= 0.7Å. There is no evidence for a significant correlation between $W_\circ$([OII]) and either radius or density, apart from the lack of strong emission-line galaxies in the densest, central regions ($\lesssim 0.1$ h^{-1} Mpc). Also, we do not measure a significant difference in the dynamics of the emission-line galaxies, relative to the rest of the population.
- Disk-dominated galaxies ($B/T < 0.4$) comprise 18±5% of the sample within the central 0.4 h^{-1} Mpc covered by our *WFPC2* images. Less than 25% (2/8) of these galaxies show significant emission. The remainder, a population of "anemic" disk galaxies, are relatively isolated, regular spiral galaxies near L^*, with smooth disks. Such galaxies are rarely found in local, field samples, but are also seen, in similar abundance, in more massive clusters (Poggianti et al. 1999).
- No galaxies in our sample have a spectrum characteristic of a post-starburst or of truncated star formation. Only four galaxies have H$\delta > 4$Å with at least 1σ significance, and all of these show nebular emission lines. Thus there is no evidence that these cluster environments act to enhance star formation activity, even temporarily.

The distribution of $W_\circ$([OII]) in these clusters is similar to that measured in the sample of Balogh et al. (1997), which is comprised of clusters approximately an order of magnitude more massive. Galaxies in both systems show low star formation rates even at projected surface densities as low as $\sim 10h^2$ Mpc^{-2}, where the fraction of spiral and irregular galaxies expected from the morphology-density relation is $\sim$ 60%. The fact that star formation rates are so low even in these low-mass structures has important implications for understanding galaxy evolution in general. The phenomenon is not likely to be driven by extreme processes, such as ram-pressure stripping, or interaction-induced starbursts, which are expected to be important only in the richest clusters. Rather it is something that operates in more commonplace environments, possibly groups in the infall regions of clusters (Kodama et al. 2001; Lewis et al. 2002). Tracing the evolution of galaxies in these groups, therefore, may shed light on the processes responsible for the observed decline in the globally-averaged star formation rate of the Universe.

ACKNOWLEDGEMENTS

We thank the referee, Chris Collins, for his expeditious report and useful suggestions which improved this paper. We are also grateful to the CNOC1 collaboration for allowing us to use their unpublished data. We acknowledge financial support from PPARC (MLB, RGB, RLD), the Royal Society (IRS), Leverhulme Trust (IRS, RLD), the Deutsche Forschungsgemeinschaft and the Volkswagen foundation (BLZ,AF). The data in this paper includes observations made with the NASA/ESA *Hubble Space Telescope* obtained at the Space Telescope Science Institute, which is operated by the Association of Universities for Research in Astronomy Inc., under NASA contract NAS 5-26555.

REFERENCES

Allen, S. W. & Fabian, A. C. 1998, MNRAS, 297, L57

Babul, A., Balogh, M. L., Lewis, G. F., & Poole, G. B. 2002, MNRAS, 330, 329

Balogh, M. L., Christlein, D., Zabludoff, A. I., & Zaritsky, D. 2001, ApJ, 557, 117

Balogh, M. L., Couch, W. J., Smail, I., Bower, R. G., & Glazebrook. 2002a, MNRAS, in press, astroph/0203334

Balogh, M. L., Morris, S. L., Yee, H. K. C., Carlberg, R. G., & Ellingson, E. 1997, ApJL, 488, 75

—. 1999, ApJ, 527, 54

Balogh, M. L., Navarro, J. F., & Morris, S. L. 2000, ApJ, 540, 113

Balogh, M. L., Schade, D., Morris, S. L., Yee, H. K. C., Carlberg, R. G., & Ellingson, E. 1998, ApJL, 504, 75

Balogh, M. L., Smail, I., Bower, R. G., Ziegler, B. L., Smith, G. P., Davies, R. L., Gaztelu, A., Kneib, J.-P., & Ebeling, H. 2002b, ApJ, 566, 123

Beers, T. C., Flynn, K., & Gebhardt, K. 1990, AJ, 100, 32

Bekki, K., Couch, W. J., & Shioya, Y. 2002, ApJ, in press, astroph/0206207

Bender, R. 1990, A&A, 229, 441

Bower, R. G. 1991, MNRAS, 248, 332

Butcher, H. & Oemler, A. 1984, ApJ, 285, 426

Carlberg, R. G., Yee, H. K. C., Ellingson, E., Abraham, R., Gravel, P., Morris, S., & Pritchet, C. J. 1996, ApJ, 462, 32

Carlberg, R. G., Yee, H. K. C., Ellingson, E., Morris, S. L., Abraham, R., Gravel, P., Pritchet, C. J., Smecker-Hane, T., Hartwick, F. D. A., Hesser, J. E., Hutchings, J. B., & Oke, J. B. 1997, ApJL, 476, L7

Charlot, S. . & Fall, S. M. 2000, ApJ, 539, 718

Charlot, S. . & Longhetti, M. 2001, MNRAS, 323, 887

Charlot, S., Kauffmann, G., Longhetti, M., Tresse, L., White, S. D. M., Maddox, S. J., & Fall, S. M. 2002, MNRAS, 330, 876

Christlein, D. 2000, ApJ, 545, 145

Couch, W. J., Balogh, M. L., Bower, R. G., Smail, I., Glazebrook, K., & Taylor, M. 2001, ApJ, 549, 820

Couch, W. J. & Sharples, R. M. 1987, MNRAS, 229, 423

Cowie, L. L., Songaila, A., & Barger, A. J. 1999, AJ, 118, 603

Crawford, C. S., Allen, S. W., Ebeling, H., Edge, A. C., & Fabian, A. C. 1999, MNRAS, 306, 857

David, L. P., Slyz, A., Jones, C., Forman, W., Vrtilek, S. D., & Arnaud, K. A. 1993, ApJ, 412, 479

de Jong, R. S. & Davies, R. L. 1997, MNRAS, 285, L1

Diaferio, A., Kauffmann, G., Balogh, M. L., White, S. D. M., Schade, D., & Ellingson, E. 2001, MNRAS, 323, 999

Domínguez, M., Muriel, H., & Lambas, D. G. 2001, AJ, 121, 1266

Dressler, A. 1980, ApJ, 236, 351

Dressler, A. & Gunn, J. E. 1983, ApJ, 270, 7

Dressler, A., Oemler, A., Couch, W. J., Smail, I., Ellis, R. S., Barger, A., Butcher, H. R., Poggianti, B. M., & Sharples, R. M. 1997, ApJ, 490, 577

Dressler, A., Smail, I., Poggianti, B. M., Butcher, H., Couch, W. J., Ellis, R. S., & Oemler, A. 1999, ApJS, 122, 51

Edge, A. C. 2001, MNRAS, 328, 762

Ellingson, E., Lin, H., Yee, H. K. C., & Carlberg, R. G. 2001, ApJ, 547, 609

Ellis, R. S., Colless, M., Broadhurst, T., Heyl, J., & Glazebrook, K. 1996, MNRAS, 280, 235

Fairley, B. W., Jones, L. R., Wake, D. A., Collins, C. A., Burke, D. J., Nichol, R. C., & Romer, A. K. 2002, MNRAS, 330, 755

Fujita, Y. 1998, ApJ, 509, 587

—. 2001, ApJ, 550, 612

Fujita, Y. & Nagashima, M. 1999, ApJ, 516, 619

Fukugita, M., Shimasaku, K., & Ichikawa, T. 1995, PASP, 107, 945

Girardi, M., Giuricin, G., Mardirossian, F., Mezzetti, M., & Boschin, W. 1998, ApJ, 505, 74

Gomez, P. L., Nichol, R. C., Miller, C. J., Balogh, M. L., Goto, T., Zabludoff, A. I., Romer, A. K., Bernardi, M., Sheth, R., Hopkins, A. M., Castander, F. J., Connolly, A., Schneider, D. P., Brinkmann, J., Lamb, D. Q., SubbaRao, M., & York, D. G. 2002, ApJ, submitted

Gunn, J. E. & Gott, J. R. 1972, ApJ, 176, 1

Jansen, R. A., Fabricant, D., Franx, M., & Caldwell, N. 2000, ApJS, 126, 331

Kauffmann, G. 1996, MNRAS, 281, 487

Kells, W., Dressler, A., Sivaramakrishnan, A., Carr, D., Koch, E., Epps, H., Hilyard, D., & Pardeilhan, G. 1998, PASP, 110, 1487

Kennicutt, R. C. 1983, ApJ, 272, 54

—. 1992, ApJ, 388, 310

Kewley, L. J., Dopita, M. A., Sutherland, R. S., Heisler, C. A., & Trevena, J. 2001, ApJ, 556, 121

Kinney, A. L., Calzetti, D., Bohlin, R. C., McQuade, K., Storchi-Bergmann, T., & Schmitt, H. R. 1996, ApJ, 467, 38

Kodama, T. & Bower, R. G. 2001, MNRAS, 321, 18

Kodama, T. & Smail, I. 2001, MNRAS, 326, 637

Kodama, T., Smail, I., Nakata, F., Okamura, S., & Bower, R. G. 2001, ApJL, 562, L9

Larson, R. B., Tinsley, B. M., & Caldwell, C. N. 1980, ApJ, 237, 692

Lewis, A. D., Ellingson, E., Morris, S. L., & Carlberg, R. G. 1999, ApJ, 517, 587

Lewis, I., Balogh, M., De Propris, R., Couch, W., Bower, R., Offer, A., Bland-Hawthorn, J., Baldry, I. K., Baugh, C., Bridges, T., Cannon, R., Cole, S., Colless, M., Collins, C., Cross, N., Dalton, G., Driver, S. P., Efstathiou, G., Ellis, R. S., Frenk, C. S., Glazebrook, K., Hawkins, E., Jackson, C., Lahav, O., Lumsden, S., Maddox, S., Madgwick, D., Norberg, P., Peacock, J. A., Percival, W., Peterson, B. A., Sutherland, W., & Taylor, K. 2002, MNRAS, 334, 673

Lilly, S. J., Le Fevre, O., Hammer, F., & Crampton, D. 1996, ApJL, 460, L1

Lin, H., Kirshner, R. P., Shectman, S. A., Landy, S. D., Oemler, A., Tucker, D. L., & Schechter, P. L. 1996, ApJ, 464, 60

Lin, H., Yee, H. K. C., Carlberg, R. G., Morris, S. L., Sawicki, M., Patton, D. R., Wirth, G., & Shepherd, C. W. 1999, ApJ, 518, 533

Madau, P., Ferguson, H. C., Dickinson, M. E., Giavalisco, M., Steidel, C., & Fruchter, A. 1996, MNRAS, 283, 1388

Markevitch, M. 1998, ApJ, 504, 27

Moore, B., Lake, G., Quinn, T., & Stadel, J. 1999, MNRAS, 304, 465

Okamoto, T. & Nagashima, M. 2001, ApJ, 547, 109

Ostrander, E. J., Nichol, R. C., Ratnatunga, K. U., & Griffiths, R. E. 1998, AJ, 116, 2644

Pimbblet, K. A., Smail, I., Kodama, T., Couch, W. J., Edge, A. C., Zabludoff, A. I., & O'Hely, E. 2002, MNRAS, 331, 333

Poggianti, B. M., Smail, I., Dressler, A., Couch, W. J., Barger, A. J., Butcher, H., Ellis, R. S., & Oemler, A. 1999, ApJ, 518, 576

Poggianti, B. M. & Wu, H. 2000, ApJ, 529, 157

Postman, M. & Geller, M. J. 1984, ApJ, 281, 95

Postman, M., Lubin, L. M., & Oke, J. B. 2001, AJ, 122, 1125

Quilis, V., Moore, B., & Bower, R. 2000, Science, 288, 1617

Ratnatunga, K. U., Griffiths, R. E., & Ostrander, E. J. 1999, AJ, 118, 86

Silva, L., Granato, G. L., Bressan, A., & Danese, L. 1998, ApJ, 509, 103

Simard, L., Willmer, C. N. A., Vogt, N. P., Sarajedini, V. L., Phillips, A. C., Weiner, B. J., Koo, D. C., Im, M., Illingworth, G. D., & Faber, S. M. 2002, ApJS, in press, astroph/0205025

Smith, G. P., Smail, I., Kneib, J.-P., Czoske, O., Ebeling, H., Edge, A. C., Pelló, R., Ivison, R. J., Packham, C., & Le Borgne, J.-F. 2002, MNRAS, 330, 1

Trager, S. C., Worthey, G., Faber, S. M., Burstein, D., & Gonzalez, J. J. 1998, ApJS, 116, 1

van den Bergh, S. 1976, ApJ, 206, 883

—. 1991, PASP, 103, 390

Veilleux, S. & Osterbrock, D. E. 1987, ApJS, 63, 295

Vikhlinin, A., McNamara, B., Forman, W., Jones, C., & Quintana, H. 1998, ApJL, 498, 21

Wilson, G., Cowie, L. L., Barger, A. J., & Burke, D. J. 2002, AJ, submitted, astroph/0203168

Xue, Y. & Wu, X. 2000, ApJ, 538, 65

Yee, H. K. C., Ellingson, E., & Carlberg, R. G. 1996, ApJS, 102, 269

Zabludoff, A. I. & Mulchaey, J. S. 1998, ApJ, 496, 39

Table 4. PROPERTIES OF CLUSTER MEMBERS

Cluster	Galaxy ID	$R_{\rm mag}$	Redshift	R.A. (J2000)	Dec (J2000)	B/T	S/N	$W_\circ$([OII]) Å	$W_\circ(H\delta)$ Å	$W_\circ(H\alpha$+[NII]) Å
Cl0818	13	20.5	0.2682	08 19 17.822	56 53 17.833	...	9.6	34.7±6.1	3.2±2.5	80.1±24.4
Cl0818	51	20.1	0.2723	08 19 19.288	56 53 56.929	...	6.4	20.5±7.4	7.9±2.4	...
Cl0818	54	19.6	0.2670	08 18 56.598	56 54 10.346	0.02	16.4	2.0±2.9	2.8±1.5	...
Cl0818	58	20.1	0.2667	08 18 52.914	56 54 25.988	0.19	7	−9.7±7.8	2.0±3.6	22.1±11.6
Cl0818	64	19.0	0.2703	08 19 02.249	56 54 28.199	...	8.6	9.4±5.5	−2.1±2.1	...
Cl0818	66	19.6	0.2698	08 18 54.792	56 54 44.158	1.00	11.8	1.0±3.7	−4.1±2.3	...
Cl0818	67	19.0	0.2688	08 19 09.943	56 54 44.773	0.77	8.8	−2.8±5.1	−2.5±3.0	...
Cl0818	86	19.7	0.2643	08 19 14.008	56 55 24.395	...	4.6	6.8±22.5	...	...
Cl0818	87	19.8	0.2643	08 18 59.467	56 55 29.078	0.24	5.4	38.2±11.3	3.9±3.0	99.9±10.0
Cl0819	2	18.5	0.2278	08 18 48.715	70 52 55.844	...	22.6	−3.3±1.5	−0.4±0.8	3.1±1.1
Cl0819	4	19.8	0.2290	08 20 29.912	70 53 06.119	...	11.4	21.6±4.0	3.3±1.4	37.9±3.4
Cl0819	6	18.5	0.2319	08 19 06.486	70 53 04.114	...	23.8	−0.4±1.5	1.0±0.7	0.8±0.9
Cl0819	9	18.7	0.2280	08 20 13.008	70 53 34.627	...	14.2	1.4±3.0	1.6±1.3	−1.3±1.3
Cl0819	11	18.7	0.2304	08 19 07.756	70 53 37.702	...	18.8	−4.6±1.8	−1.0±1.0	−0.6±1.0
Cl0819	12	18.7	0.2309	08 19 37.969	70 53 49.513	...	16.4	−1±2.5	−1.3±1.1	0.6±1.1
Cl0819	13	18.4	0.2294	08 19 46.923	70 53 53.855	...	20	6.1±2.5	...	...
Cl0819	15	18.7	0.2305	08 19 35.251	70 54 02.423	...	19	−4.6±2.1	−0.4±1.0	1.8±1.0
Cl0819	16	18.4	0.2320	08 19 04.374	70 53 54.953	0.75	24.2	−1.8±1.5	0.6±0.7	5.1±0.9
Cl0819	20	19.1	0.2305	08 20 12.887	70 54 29.862	...	14.6	1.9±2.6	3.0±1.2	11.2±1.7
Cl0819	21	18.3	0.2272	08 19 42.125	70 54 32.087	...	25.4	−2.5±1.5	−1.0±0.7	−0.1±0.8
Cl0819	25	19.2	0.2296	08 18 56.120	70 54 39.445	...	13.4	−2.5±2.8	1.2±1.3	...
Cl0819	26	19.7	0.2280	08 19 22.859	70 54 44.914	...	5.4	−5.8±6.4	−1.0±4.5	...
Cl0819	27	19.0	0.2277	08 19 01.384	70 54 51.642	0.52	15.4	−3.9±2.3	−0.1±1.2	−1.6±1.5
Cl0819	29	19.2	0.2297	08 18 54.033	70 54 52.628	...	18	14.1±2.2	3.7±0.9	29.8±2.2
Cl0819	33	18.6	0.2289	08 19 17.747	70 55 00.952	...	16.6	−5.6±2.5	0.8±1.1	−0.2±1.0
Cl0819	34[a]	17.9	0.2304	08 19 18.340	70 55 04.411	...	34.8	−1.8±1.0	0.5±0.5	1.1±0.6
Cl0819	36	19.4	0.2304	08 19 23.751	70 55 24.272	...	11.6	−0.9±3.7	1.7±1.6	−3.3±1.6
Cl0819	37	19.0	0.2310	08 19 05.949	70 55 34.460	0.44	9.2	−6.2±4.1	2.6±2.5	...
Cl0819	40	18.4	0.2274	08 19 11.986	70 55 43.828	...	23.4	−0.4±1.6	0.0±0.8	0.8±0.9
Cl0819	43	19.1	0.2313	08 19 12.638	70 56 05.798	...	14.4	−2±2.7	0.9±1.3	0.7±1.3
Cl0819	44	19.9	0.2301	08 20 09.086	70 56 17.527	...	10.6	22.0±4.3	2.8±1.6	64.9±6.0
Cl0819	47	18.2	0.2306	08 19 23.597	70 56 30.764	0.66	26.6	−4±1.5	−0.5±0.7	0.9±0.8
Cl0841	4	19.4	0.2403	08 42 17.150	70 45 21.892	...	8.8	−0.3±4.2	1.7±2.0	4.5±1.9
Cl0841	10	20.0	0.2362	08 41 09.943	70 45 43.974	...	10.4	9.7±3.5	2.9±1.6	27.6±3.3
Cl0841	14	20.2	0.2423	08 41 43.495	70 46 24.265	0.78	7	−2.7±5.1	2.8±2.4	−2.7±2.6
Cl0841	15	19.1	0.2397	08 41 46.827	70 46 28.524	0.89	15.4	0.8±2.6	−0.2±1.2	−2.5±1.1
Cl0841	16	19.3	0.2403	08 41 47.226	70 46 31.627	0.91	11	1.9±3.9	−0.3±1.7	−4.1±1.5
Cl0841	20	18.3	0.2372	08 41 37.445	70 46 55.657	0.42	29.8	0.2±1.2	−0.0±0.6	−1.5±0.6
Cl0841	23	19.6	0.2396	08 41 14.286	70 46 59.340	...	16.4	14.8±2.3	4.3±1.0	42.5±2.5
Cl0841	24	20.0	0.2415	08 41 41.982	70 46 54.095	0.86	5.2	4.8±7.5	1.4±3.5	−4.2±3.1
Cl0841	25[a]	17.9	0.2397	08 41 44.081	70 46 52.748	0.46	29.8	1.8±1.9	−1.4±0.6	−2.7±0.6
Cl0841	27	20.6	0.2384	08 41 40.979	70 47 15.598	0.63	4	13.6±13.4	3.7±4.3	−4.2±3.9
Cl0841	28	19.9	0.2367	08 41 04.120	70 47 15.572	...	9.4	−5.2±4.0	2.5±1.8	0.0±2.1
Cl0841	30	20.5	0.2396	08 41 54.499	70 47 31.308	...	6.6	20.6±6.1	−0.7±2.8	36.0±5.8
Cl0841	33	19.7	0.2401	08 41 25.184	70 47 45.895	...	10.4	−9.1±3.3	0.1±1.7	−3.4±1.7
Cl0841	34	19.2	0.2388	08 41 28.476	70 47 47.350	...	14.2	−1±2.8	0.5±1.3	3.0±1.3
Cl0841	37	18.7	0.2373	08 41 30.923	70 47 52.732	0.55	21.6	−1.6±1.7	0.1±0.8	6.4±0.9
Cl0841	38	18.1	0.2402	08 41 32.395	70 47 57.401	0.82	34	11.7±1.2	2.0±0.5	10.6±0.7
Cl0841	41	18.8	0.2415	08 40 48.377	70 48 26.352	...	19.6	0.5±2.0	0.7±0.9	−2.1±1.0
Cl0841	44	19.3	0.2396	08 41 50.230	70 48 43.243	0.63	10.4	−2.3±3.8	0.6±1.8	−4.5±1.8
Cl0841	46	19.8	0.2387	08 41 54.697	70 48 53.240	0.90	7	−10.1±5.8	0.6±2.6	1.6±2.8
Cl0841	50	19.9	0.2400	08 42 47.915	70 49 08.648	...	5.8	−3.3±5.9	0.4±3.0	12.6±3.6
Cl0841	51	19.5	0.2418	08 40 52.291	70 49 17.299	...	9.8	19.3±5.1	1.6±2.3	118.3±64.2
Cl0849	6	19.2	0.2346	08 49 15.608	37 28 14.408	...	9	...	−4.5±2.2	1.4±2.0
Cl0849	12	19.5	0.2295	08 49 07.537	37 29 00.082	...	8.2	−0.8±7.1	3.0±3.0	...
Cl0849	20	19.9	0.2382	08 49 07.650	37 30 25.679	0.90	5.6	13.3±9.5	6.4±3.2	...
Cl0849	21	18.7	0.2375	08 49 06.456	37 30 37.134	...	13.2	1.6±2.8	2.0±1.3	6.1±1.5
Cl0849	22	19.3	0.2347	08 49 06.888	37 30 47.131	0.35	5.2	15.8±7.6	−0.2±3.5	40.1±6.4
Cl0849	23	19.4	0.2315	08 49 09.719	37 30 59.368	0.83	5	0.6±7.2	3.4±3.5	1.0±4.5
Cl0849	24[a]	17.9	0.2370	08 49 10.759	37 31 09.023	0.49	23	0.5±1.5	0.2±0.8	−0.2±0.7

Table 4. continued

Cluster	Galaxy ID	$R_{\rm mag}$	Redshift	R.A.	Dec	B/T	S/N	$W_\circ$([OII])	$W_\circ(H\delta)$	$W_\circ(H\alpha$+[NII])
				(J2000)				Å	Å	Å
Cl0849	25	19.1	0.2310	08 49 10.506	37 31 14.898	0.47	5.8	0.7±6.4	1.0±3.1	2.2±4.4
Cl0849	26	18.3	0.2385	08 49 10.975	37 30 52.556	0.71	18	−1.2±2.2	−1.2±1.1	−0±1.0
Cl0849	27	18.6	0.2403	08 49 09.152	37 31 23.484	...	16.4	0.3±2.4	2.8±1.1	−2.8±1.2
Cl0849	29	18.5	0.2290	08 49 12.967	37 31 49.714	...	16.6	−0.9±2.3	0.9±1.1	...
Cl0849	34	19.0	0.2382	08 49 08.738	37 32 30.113	0.75	10.4	−2.5±4.0	2.1±1.7	−1.1±1.7
Cl0849	35	19.1	0.2391	08 49 11.554	37 32 37.036	...	7.2	−1.6±4.9	0.1±2.4	−1.6±3.1
Cl0849	37	19.7	0.2315	08 49 08.189	37 33 49.010	...	5	0.6±7.2	3.4±3.5	1.0±4.5
Cl0849	38	18.6	0.2335	08 49 00.132	37 33 53.186	...	13.6	−0.1±2.7	−1.4±1.4	1.2±1.5
Cl0849	39	18.4	0.2339	08 49 10.045	37 34 02.564	...	11.6	0.2±2.8	−1.2±1.6	3.1±1.9
Cl0849	40	19.5	0.2315	08 49 08.437	37 34 05.214	...	6.2	3.6±7.1	1.3±3.0	...
Cl0849	42	18.7	0.2318	08 49 09.584	37 34 18.426	...	12.4	−3.7±3.2	−1.5±1.5	0.4±1.5
Cl0849	45	19.5	0.2321	08 49 11.096	37 34 31.570	...	6.4	3.6±7.6	−3.0±3.0	5.6±3.1
Cl0849	46	19.7	0.2320	08 49 20.768	37 34 44.202	...	5.2	1.8±9.3	1.0±3.4	−1.5±4.0
Cl0849	50	19.0	0.2326	08 49 00.897	37 34 59.570	...	10.2	−4.5±4.6	−0.4±1.8	−1.1±1.9
Cl0849	52	19.9	0.2343	08 49 19.087	37 35 24.576	...	6.2	14.6±8.1	3.6±2.8	23.9±5.5
Cl0849	53	19.0	0.2346	08 49 04.545	37 35 44.873	...	12	−4.5±3.2	0.2±1.5	...
Cl0849	54	19.4	0.2337	08 49 13.623	37 36 00.119	...	8.2	−9.2±5.4	−2.0±2.4	−5.4±2.4
Cl0849	56	19.3	0.2356	08 49 09.393	37 36 12.438	...	8.6	−2.5±4.1	1.0±2.1	1.1±2.6
Cl0849	-99	19.8	0.2309	08 49 09.635	37 35 42.871	...	6	−4.2±6.3	1.5±3.0	−0.1±4.4
Cl1309	48	19.7	0.2998	13 10 02.322	32 21 12.229	...	11	11.3±3.2	5.9±1.4	26.9±4.3
Cl1309	59	19.6	0.2961	13 10 06.826	32 21 22.957	...	7	−3.9±4.7	0.2±2.5	...
Cl1309	75	19.8	0.2907	13 10 04.200	32 21 34.204	...	6.2	−2.9±5.0	3.2±2.6	−3.2±4.9
Cl1309	81	19.8	0.2991	13 09 59.128	32 21 43.981	...	4	3.4±12.0	−0.2±4.1	...
Cl1309	83	19.2	0.2934	13 09 55.063	32 21 45.752	0.39	9	−2.7±4.0	−3.9±2.0	...
Cl1309	99	19.5	0.2996	13 09 53.225	32 21 56.326	0.80	6.4	−3.3±5.4	1.6±2.6	0.7±3.8
Cl1309	118	19.0	0.2930	13 10 11.341	32 22 01.092	...	11	−5.9±2.9	0.0±1.6	...
Cl1309	119	20.4	0.2977	13 09 53.093	32 22 10.801	0.26	3.4	...	...	−12.1±6.8
Cl1309	133	19.0	0.2927	13 09 51.577	32 22 14.070	...	9.4	−5.3±3.1	−2.3±1.9	1.1±2.7
Cl1309	142	19.8	0.2939	13 09 55.177	32 22 24.560	0.70	5	0.6±7.5	−0.8±3.5	...
Cl1309	151[a]	18.4	0.2930	13 09 56.118	32 22 13.822	0.57	19.2	−5.2±1.7	−1.4±0.9	3.2±1.3
Cl1309	155	19.0	0.2934	13 09 58.502	32 22 28.668	0.73	10.8	−3±3.1	...	...
Cl1309	165	19.0	0.2945	13 10 13.066	32 22 49.667	...	11.2	−1.2±2.7	−0.0±1.6	...
Cl1309	174	19.4	0.2925	13 10 00.194	32 22 57.464	...	12.8	6.3±2.5	5.1±1.2	13.6±3.3
Cl1309	190	19.2	0.2913	13 09 56.349	32 23 08.066	0.47	5.4	5.0±6.1	1.2±3.1	18.5±5.4
Cl1309	191	19.9	0.2913	13 10 09.016	32 23 10.950	...	5	3.6±8.6	−0.7±3.5	−5.5±5.1
Cl1309	193	19.0	0.2927	13 09 57.689	32 23 10.525	0.62	11	2.7±3.3	−1.8±1.6	3.0±2.3
Cl1309	199	21.1	0.2933	13 09 42.056	32 23 29.558	...	4.2	15.4±7.7	−1.0±4.3	97.5±31.9
Cl1309	214	20.3	0.2942	13 09 45.026	32 23 31.866	...	7.8	7.5±4.1	2.8±2.1	...
Cl1444a	74	19.5	0.2916	14 43 32.384	63 45 15.188	...	6.8	−2.4±5.7	−0.6±2.5	...
Cl1444a	78	19.1	0.2899	14 43 54.807	63 45 13.885	0.42	12	3.5±2.7	...	...
Cl1444a	80	18.2	0.2918	14 44 04.940	63 45 06.124	...	17.6	−3±1.9	−0.9±1.0	...
Cl1444a	84	19.4	0.2921	14 43 46.399	63 45 16.726	...	7.6	4.6±5.2	0.5±2.3	...
Cl1444a	89	19.4	0.2950	14 43 09.283	63 45 23.346	...	8.4	3.5±4.1	0.5±2.1	...
Cl1444a	93	19.8	0.2920	14 44 15.062	63 45 23.468	0.00	8.6	1.7±3.8	4.4±1.9	15.2±8.4
Cl1444	100	18.7	0.2908	14 44 23.851	63 45 29.966	...	14	0.1±2.5	3.3±1.2	...
Cl1444	107	19.3	0.2949	14 43 50.343	63 45 41.130	...	10	5.0±3.3	3.1±1.6	15.0±4.1
Cl1444	110[a]	18.0	0.2908	14 43 54.997	63 45 34.812	0.63	23	0.1±1.5	0.7±0.8	...
Cl1444	111	19.6	0.2902	14 44 01.033	63 45 41.612	...	6.6	1.1±4.8	1.3±2.5	...
Cl1444a	115	19.0	0.2921	14 44 00.945	63 45 48.888	...	13.2	−2.6±2.6	...	...
Cl1444a	121	19.2	0.2935	14 43 32.725	63 46 00.700	...	11.2	9.9±3.6	4.8±1.4	6.2±2.5
Cl1444	149	19.0	0.2951	14 43 16.978	63 46 37.916	...	10.2	−3.3±3.3	−1.3±1.7	...
Cl1444a	170	19.1	0.2964	14 43 36.859	63 47 18.758	...	12.2	5.2±2.9	4.7±1.3	13.2±2.6
Cl1444a	89	19.4	0.2950	14 43 09.283	63 45 23.346	...	8.4	3.5±4.1	0.5±2.1	...
Cl1444a	149	19.0	0.2951	14 43 16.978	63 46 37.916	...	10.2	−3.3±3.3	−1.3±1.7	...
Cl1444a/b	170	19.1	0.2964	14 43 36.859	63 47 18.758	...	12.2	5.2±2.9	4.7±1.3	13.2±2.6
Cl1444b	24	18.8	0.2976	14 44 34.578	63 43 12.349	...	11	7.8±3.5	−0.7±1.6	...
Cl1444b	28	19.9	0.2976	14 43 25.496	63 43 43.756	...	4.6	...	−0.7±3.8	...
Cl1444b	59	18.7	0.3000	14 44 24.272	63 44 37.381	...	11.6	...	1.0±1.5	...
Cl1444b	62	19.0	0.3014	14 44 06.299	63 44 57.185	...	12.6	−1±2.8	−0.9±1.4	...
Cl1444b	70	18.8	0.3009	14 43 53.020	63 45 07.002	0.68	16.8	−3.8±1.9	0.4±1.0	...

Table 4. continued

Cluster	Galaxy ID	$R_{\rm mag}$	Redshift	R.A.	Dec	B/T	S/N	$W_\circ([\text{O II}])$	$W_\circ(H\delta)$	$W_\circ(H\alpha+[\text{N II}])$
				(J2000)				Å	Å	Å
Cl1444b	71[a]	18.4	0.2986	14 44 06.852	63 44 58.722	...	13.4	1.3±2.5	−0.7±1.3	...
Cl1444b	75	18.2	0.3010	14 43 47.029	63 45 08.474	...	22.8	−6.2±1.4	−0.7±0.8	...
Cl1444b	79	20.1	0.3017	14 43 53.265	63 45 16.067	0.56	4.4	2.6±6.3	0.8±4.0	...
Cl1444b	85	19.3	0.2986	14 43 57.990	63 45 16.934	0.34	7	3.3±4.6	−2.7±2.6	...
Cl1444b	86	20.2	0.2994	14 44 40.067	63 45 10.246	...	3.6	4.4±11.7	1.3±4.8	...
Cl1444b	113	20.4	0.3023	14 44 09.141	63 45 46.721	1.00	3.6	−11.1±7.8	3.1±4.9	...
Cl1444b	122	19.7	0.3045	14 43 40.895	63 46 02.305	...	5.8	13.3±6.1	−3.1±3.2	7.5±6.1
Cl1444b	138	19.2	0.3017	14 43 57.286	63 46 18.332	0.77	12.2	−5.7±2.6	1.0±1.5	−0.6±2.1
Cl1444b	157	18.8	0.3001	14 44 02.710	63 46 56.017	0.82	14.6	−2.4±2.5	0.2±1.2	...
Cl1444b	166	19.9	0.3032	14 43 38.507	63 47 15.475	...	6	9.1±7.0	10.2±2.7	22.6±6.0
Cl1633	1	19.8	0.2373	16 33 28.890	57 12 10.577	...	11.6	−0±4.1	4.5±2.0	...
Cl1633	9	20.9	0.2412	16 33 29.194	57 13 37.340	...	3.4	−7.6±9.3	1.5±5.3	...
Cl1633	13	19.9	0.2450	16 33 16.311	57 14 04.877	...	12.6	44.2±3.7	3.4±1.3	50.4±5.9
Cl1633	14	20.1	0.2388	16 33 35.339	57 14 04.218	0.82	6.6	−4.8±5.1	−1.6±2.7	−6.8±3.5
Cl1633	15	19.8	0.2417	16 33 42.836	57 14 02.378	0.62	5.4	3.2±9.5	−3.0±5.0	...
Cl1633	17	20.2	0.2402	16 33 40.276	57 14 11.522	0.77	5	4.9±12.7	−2.6±5.3	...
Cl1633	22	19.1	0.2388	16 33 41.726	57 14 20.436	0.75	10.2	−11.5±4.7	−0.2±2.5	...
Cl1633	23	20.6	0.2422	16 33 43.374	57 14 27.013	0.77	4.6	0.1±6.8	1.0±3.9	0.4±7.2
Cl1633	24	21.0	0.2417	16 33 14.114	57 14 33.799	...	4.2	46.3±12.2	−4.2±4.7	45.7±18.5
Cl1633	25[a]	18.4	0.2402	16 33 42.129	57 14 12.649	0.56	18	−2.3±1.7	−1.0±1.0	...
Cl1633	27	19.8	0.2396	16 33 31.879	57 14 31.517	...	7.6	−2.2±4.9	0.5±2.4	0.0±3.1
Cl1633	28	20.3	0.2371	16 33 30.890	57 14 31.585	...	9	16.9±6.5	−0.4±2.9	...
Cl1633	31	19.4	0.2425	16 33 41.155	57 14 29.281	0.71	9.8	−5.3±3.4	−2.8±1.9	...
Cl1633	34	19.1	0.2407	16 33 05.867	57 14 52.379	...	13	−0.4±2.8	0.0±1.4	...
Cl1633	35	19.2	0.2366	16 33 50.398	57 14 46.705	...	12.6	1.0±2.8	−0.0±1.5	...
Cl1633	43	20.7	0.2404	16 33 39.426	57 15 14.144	0.43	4.2	−1.5±7.7	−0.0±4.5	...
Cl1633	46	18.8	0.2384	16 33 24.291	57 15 11.686	...	18.4	5.3±1.9	2.3±1.0	...
Cl1633	47	19.2	0.2394	16 33 56.034	57 15 23.566	...	12.6	−3.9±2.7	0.2±1.5	...
Cl1701	42	20.1	0.2464	17 01 59.839	64 19 21.036	...	5.6	5.2±6.2	3.8±2.7	13.8±4.9
Cl1701	86	19.5	0.2480	17 01 25.239	64 20 14.593	...	6.8	4.0±5.5	3.8±2.3	4.5±3.1
Cl1701	102	19.4	0.2422	17 01 27.279	64 20 47.692	...	13.6	30.4±3.1	5.3±1.2	53.2±3.7
Cl1701	116	19.7	0.2460	17 02 17.212	64 20 59.114	...	6.6	3.3±7.0	0.7±2.7	−4.1±2.5
Cl1701	118	19.8	0.2475	17 01 49.471	64 21 08.316	0.65	6.2	5.0±7.5	...	−6.7±2.5
Cl1701	120	19.3	0.2428	17 01 56.814	64 21 02.549	1.00	8.6	−0.9±4.1	1.3±2.0	−2.8±2.1
Cl1701	122	19.1	0.2451	17 01 36.610	64 21 07.960	...	11.8	5.7±3.5	0.9±1.5	7.8±1.7
Cl1701	123[a]	18.4	0.2457	17 01 47.754	64 21 00.133	0.86	18.6	−2.2±1.9	−1.4±1.0	−4.8±1.0
Cl1701	124	18.4	0.2408	17 01 46.794	64 20 57.304	0.48	16.6	0.7±2.3	−1.0±1.1	−0.3±0.9
Cl1701	127	19.2	0.2411	17 02 06.423	64 21 12.629	...	8.4	−0.9±4.3	3.5±2.0	...
Cl1701	141	19.0	0.2429	17 01 51.826	64 21 32.677	0.38	11.6	43.1±4.8	−0.5±1.5	19.2±1.6
Cl1701	149	19.3	0.2458	17 01 42.825	64 21 49.460	0.28	11.4	3.8±3.2	4.6±1.4	23.4±2.5
Cl1702	14	19.2	0.2193	17 02 43.737	64 18 05.504	...	9.8	3.4±4.6	−0.8±1.8	10.3±2.5
Cl1702	22	20.3	0.2233	17 02 23.804	64 18 36.155	...	3.8	−12.4±10.4	3.4±4.5	1.6±6.6
Cl1702	28	18.6	0.2250	17 01 56.744	64 18 40.219	...	17.2	3.6±2.1	0.3±1.0	8.0±1.1
Cl1702	35	18.2	0.2225	17 01 40.986	64 18 56.372	...	21	−1.6±1.9	0.4±0.8	−0.5±0.8
Cl1702	41	19.4	0.2233	17 01 40.272	64 19 19.855	...	7.6	1.1±5.0	3.0±2.1	−0.3±2.7
Cl1702	60	19.3	0.2233	17 02 13.978	64 19 45.426	0.95	8	−10.2±4.5	−1.8±2.2	...
Cl1702	66	19.0	0.2225	17 02 08.958	64 19 51.852	...	9	...	−0.0±1.9	...
Cl1702	72	18.7	0.2212	17 02 14.817	64 19 46.412	0.76	10.4	2.7±3.5	1.2±1.7	4.7±1.9
Cl1702	81[a]	17.6	0.2230	17 02 13.923	64 19 53.555	0.58	38.4	−1.4±1.0	−0.4±0.5	−1.4±0.5
Cl1702	87	19.3	0.2257	17 02 09.499	64 20 14.896	...	9.2	−1.1±4.6	1.3±1.9	0.9±1.9
Cl1702	90	18.0	0.2219	17 02 06.892	64 20 07.451	...	22.4	−0.3±1.8	−0.2±0.8	−1.7±0.8
Cl1702	129	18.5	0.2238	17 02 31.282	64 21 09.526	...	9.2	−3.7±3.9	3.3±1.8	...
Cl1702	130	18.6	0.2236	17 01 36.647	64 21 15.678	...	15.2	0.9±2.6	−1.8±1.2	−3.8±1.3
Cl1702	138	19.7	0.2243	17 02 04.065	64 21 37.210	...	7.4	−4.1±5.1	−1.2±2.5	−4.1±2.6
Cl1702	143	18.4	0.2224	17 02 01.652	64 21 38.531	...	18.8	−1.3±2.1	0.7±0.9	...

[a] Central, giant elliptical galaxy.